ELUCIDATING THE MITOCHONDRIAL ARCHITECTURE OF BRANCHED-CHAIN AMINO ACID METABOLISM ENZYMES: IMPLICATIONS FOR TREATMENT

by

Stephen Paul McCalley

BS Biology, University of Pittsburgh, 2013

Submitted to the Graduate Faculty of

the Department of Human Genetics in

the Graduate School of Public Health in partial fulfillment

of the requirements for the degree of

Doctor of Philosophy

University of Pittsburgh

2018

UNIVERSITY OF PITTSBURGH

GRADUATE SCHOOL OF PUBLIC HEALTH

This dissertation was presented

by

Stephen Paul McCalley

It was defended on

February 23, 2018

and approved by

Eric S Goetzman, PhD, Associate Professor, Human Genetics
Graduate School of Public Health, University of Pittsburgh

Candace Kammerer, PhD, Associate Professor, Human Genetics
Graduate School of Public Health, University of Pittsburgh

Zsolt Urban, PhD, Associate Professor, Human Genetics
Graduate School of Public Health, University of Pittsburgh

Dissertation Advisor: Jerry Vockley, MD, PhD, Professor, Human Genetics
Graduate School of Public Health, University of Pittsburgh

Jerry Vockley, MD, PhD

ELUCIDATING THE MITOCHONDRIAL ARCHITECTURE OF BRANCHED-CHAIN AMINO ACID METABOLISM ENZYMES: IMPLICATIONS FOR TREATMENT

Stephen Paul McCalley, PhD

University of Pittsburgh, 2018

ABSTRACT

Branched chain amino acid (BCAA) metabolism occurs within the mitochondrial matrix and is comprised of 17 enzymes, some shared, organized into three pathways for the catabolism of leucine, isoleucine, and valine (LEU, ILE, and VAL respectively). However, the physical relationships of the various enzymes in the pathways are unknown. Diseases such as isovaleric academia, propionic and methylmalonic acidemias, and maple syrup urine disease are among the disorders caused by genetic deficiencies of BCAA metabolism.

I examined the BCAA pathways and their physical interactions *in vitro* through proteomics analysis and *in situ* using stimulated emission depletion microscopy. The functional interactions of the pathways were measured by flux analysis with labeled LEU, ILE, and VAL in patient and wild type cell lines, with quantification of the labeled metabolic end-products of each pathway. I examined novel potential treatments for propionic acidemia patient derived cell lines, quantitating protein, ROS production, and mitochondrial mass response to therapeutic agents.

My proteomic and imaging studies are consistent with the existence of one or more energetically favorable, metabolite-channeling BCAA super-complex(es). Flux studies demonstrate that the end products of LEU, ILE and VAL metabolism are generated in both wild type and patient derived cells lines, implying cross-talk of BCAA pathways, and a close proximity of shared enzymes. Additionally, I found that the end-product of ILE and VAL,

propionyl-CoA, does not readily enter the TCA cycle, as previously thought, while propionyl-CoA from odd chains fats does. Finally, propionyl-CoA carboxylase (PCC) deficient cell lines showed improved mitochondrial function when treated with a cardiolipin binding protein that stabilizes the inner mitochondrial membrane in cell cultures. PCC protein amount was slightly increased in treated patient cells, and ROS and mitochondrial mass was significantly decreased.

These results provide novel insight into BCAA metabolism and offer new opportunities for the development of therapeutic agents for their defects. Furthermore, because propionyl-CoA derived from odd-chain fatty acids does, in fact, readily enter the TCA cycle, results from the metabolic flux studies will impact public health by changing potential therapies used to replenish the TCA cycle intermediates for disorders of fatty acid oxidation as well as BCAA metabolism.

TABLE OF CONTENTS

LIST OF TABLES

LIST OF FIGURES

PREFACE

When I started this project, it seemed impactful, interesting, and, quite frankly, easy. While this project is still impactful and interesting, the adjective I would use to describe this project the best would be "difficult." Throughout this perceived difficulty that I have experienced, I have had the great fortune of having many people to help me along the way.

The first and foremost mention of gratitude and appreciation goes to my mentor, Dr. Jerry Vockley. I literally could not have done any of this without him. His passion for science is infectious and his ability to inspire is something I will always take with me. He has offered support for my project in various and uncountable ways, and I am proud to be a part of his lab.

The next greatest thanks have to go to my thesis committee. Their advice and suggestions turned this thesis into something great. Eric, Candy, and Zsolt have been great mentors and teachers throughout the years.

To my coworkers who have taught me so much, I hope this thesis can be evidence of your abilities to teach and motivate. I would like to thank specifically: Dr. Yudong Wang for training me when I first started; Dr. Walid Mohsen and Anu Karunanidhi, the center and lab directors, for helping me plan and execute my experiments; Shrabani Basu from the Vockley lab and Mike Calderon and everyone at the CBI who had been so helpful and friendly getting STED

images; Dr. Bingjuan Han from China who helped turn this project into a translational research venture; and anyone else in the Vockley lab that I do not have space to thank here – thank you!

Finally, I would like to thank my parents, family, and friends for offering mostly emotional support throughout my time in the Human Genetics department. I could always count on my friends and family to be there on both the "good science days" and the "bad science days," and I am forever grateful.

LIST OF ABBREVIATIONS

3MCC – 3-methylcrotonyl-CoA carboxylase; including alpha and beta subunits labeled

as MCCC1 and MCCC2

ACAD – acyl-CoA dehydrogenase

BCAA – branched chain amino acids

BCKDH – branched chain alpha keto dehydrogenase complex; including alpha and beta

subunits labeled as BCKDHA and BCKDHB

BNGE – blue native gel electrophoresis

BM(PEG)$_3$ – 1,11-bis(maleimido)triethylene glycol; a cross-linker

BSA – bovine serum albumin

PBS – phosphate buffered saline

DMEM – Dulbecco's modification of Eagle's medium

DSA – Donkey serum albumin

EGS – ethylene glycolbis(succinimidylsuccinate); a cross-linker

ETC – electron transport chain

FAO – fatty acid oxidation; FAOD – fatty acid oxidation disorders

FBS – fetal bovine serum

GLN - glutamine

IBD – isobutyryl-CoA dehydrogenase

IF – immunofluorescence

ILE – isoleucine

IVA – isovaleric acidemia

IVD – isovaleryl-CoA dehydrogenase

LCSMCC – Succinimidyl-4-(N-maleimidomethyl)cyclohexane-1-carboxy-(6-

amidocaproate); a cross-linker

LEU - leucine

MMA – methylmalonic acidemia

MSUD – maple syrup urine disease

MUT – methylmalonyl-CoA mutase

Native-PAGE – non-denaturing gel electrophoresis

PBB – phosphate buffered saline containing 2% BSA

PCC – propionyl-CoA carboxylase; including alpha and beta subunits labeled as PCCA

and PCCB

PPA – propionic acidemia

RT – room temperature

SBCAD – short-branched chain acyl-CoA dehydrogenase

SDS-PAGE – sodium dodecyl sulfate polyacrylamide gel electrophoresis

STED – stimulated emission depletion

Sulfo-EGS – a water-soluble version of EGS cross-linker

TCA – tricarboxylic acid

VAL – valine

1.0 INTRODUCTION

1.1 BCAA METABOLISM AND RELATED DISORDERS

Catabolism of the essential branched chain amino acids (BCAA) leucine, isoleucine, and valine (LEU, ILE, and VAL, respectively) begins with transport into mitochondria, followed by deamination to their 2-oxo-branched chain organic acids, then oxidative decarboxylation to form branched chain acyl coenzyme A (CoA) products[1,2]. This is accomplished through a set of transporters and enzymes common to all three amino acids. More detail about the individual BCAA enzymes is reviewed below. Thereafter, the pathways diverge (Figures 1–4). Defects in these pathways cause 15 known metabolic disorders termed branched chain organic acidurias[1,2]. These disorders are numbered in Figure 1 below. Among the most common of these disorders are those of the acyl-CoA dehydrogenases (ACADs) specific to LEU, ILE, and VAL: isovaleryl-CoA dehydrogenase (IVD), short/branched chain acyl-CoA dehydrogenase (SBCAD, also known as 2-methylbutyryl-CoA dehydrogenase), and isobutyryl-CoA dehydrogenase (IBD), respectively[3]. ACADs are a family of related enzymes active in fatty acid and branched chain amino acid oxidation that catalyze the α,β-dehydrogenation of acyl-CoA esters, transferring electrons to electron transferring flavoprotein (ETF)[4]. Biochemical and immunological studies have previously identified nine distinct members of this enzyme family, with each accepting a narrow range of substrates[5,6,7,8,9,10,11,12,13,14]. IVD is relatively specific towards the leucine

metabolite isovaleryl-CoA, while SBCAD and IBD are more promiscuous, showing some activity towards each other's substrates, 2-methylbutyryl-CoA and isobutyryl-CoA, respectively. Throughout this project, a strong emphasis will be placed on the most clinically relevant enzymes in the pathway: the branched chain alpha keto dehydrogenase (BCKDH) complex, the ACADs, 3-methylcrotonyl-CoA carboxylase (3MCC), propionyl-CoA carboxylase (PCC), and methylmalonyl-CoA mutase (MUT).
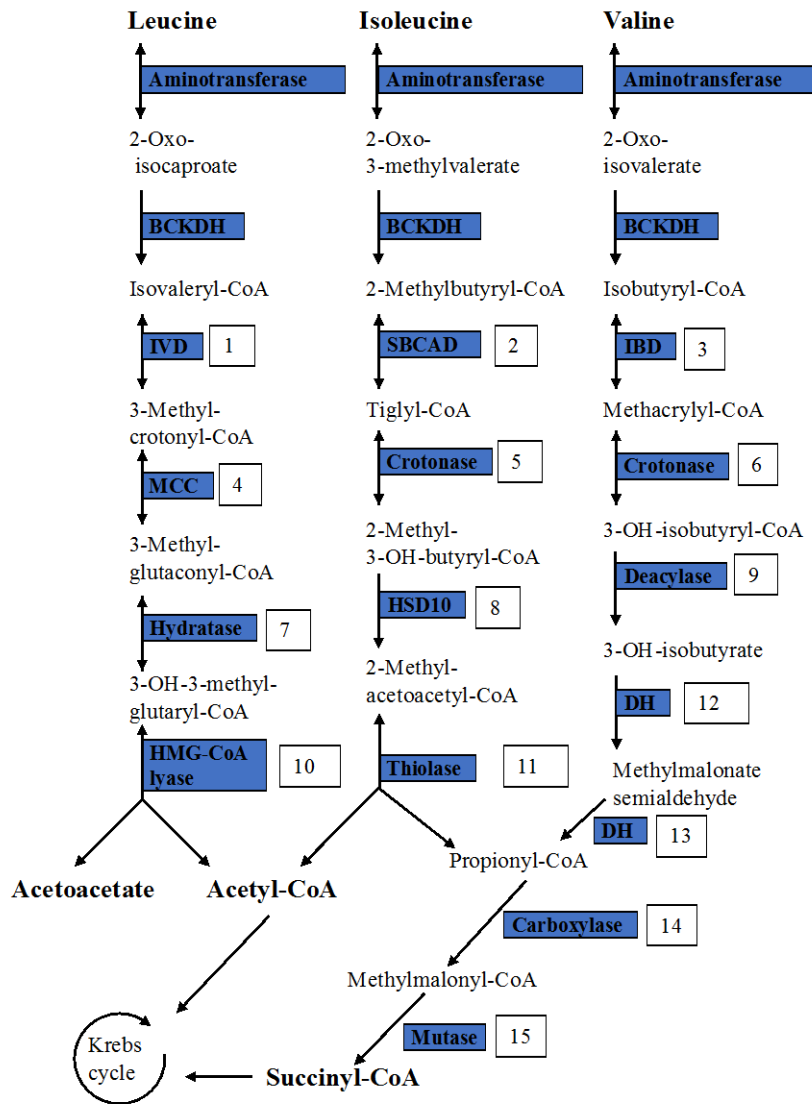
Figure 1. Overall BCAA metabolism.

Enzymes of BCAA catabolism are boxed in blue and known organic acidurias are numbered. For the purposes of this thesis, a large emphasis will be placed on 1:IVD, 2:SBCAD, 3:IBD, 4:3MCC, 14:PCC, and 15:MUT as they are among the most relevant clinically and historically.

GENE(S) ENZYME METABOLITES

L-Leucine

BCAT1, BCAT2 — Aminotransferase

2-Oxo-Isocaproate

BCKDHA, BCKDHB, DBT, DLD — Branched Chain 2-Oxo Acid Dehydrogenase

Isovaleryl-CoA

IVD — Isovaleryl-CoA Dehydrogenase

Isovaleric Acid
Isovalerylglycine
3-Hydroxyisovaleric Acid
4-Hydroxyisovaleric Acid
Mesaconic Acid
Methylsuccinic Acid
Isovaleryglucuronide
Isovalerylglutamic Acid
Isovalerylalanine
Isovalerylsarcosine
3-Hydroxyisoheptanoic Acid
Isovalerylcarnitine

3-Methylcrotonyl-CoA

3-Methylcrotonic Acid
3-Methylcrotonylglycine
3-Hydroxyisovaleric Acid
3-Hydroxyisovalerylcarnitine

MCCC1, MCCC2 — 3-Methylcrotonyl-CoA Carboxylase

3-Methylglutaconyl-CoA

3-Methylglutaconic Acid
3-Methylglutaric Acid
3-Methylglutarylcarnitine

AUH — 3-Methylglutaconyl-CoA Hydratase

3-Hydroxy-3-Methylglutaryl-CoA

3-Hydroxy-3-Methylglutaric Acid
3-methylcrotanylglycine

HMGCL — 3-Hydroxy-3-Methylglutaryl-CoA Lyase

3-Hydroxy-3-Methylglutaryl-CoA Reductase

Acetoacetate **Acetyl-CoA** **Mevalonic Acid** --→ Mevalonolactone

Cholesterol

Figure 2. LEU catabolism.

Enzymes involved in LEU catabolism are listed in blue and their relative genes are listed in green (left). Alternate metabolites generated by BCAAs are listed in red (right) at their relative steps in the pathway.
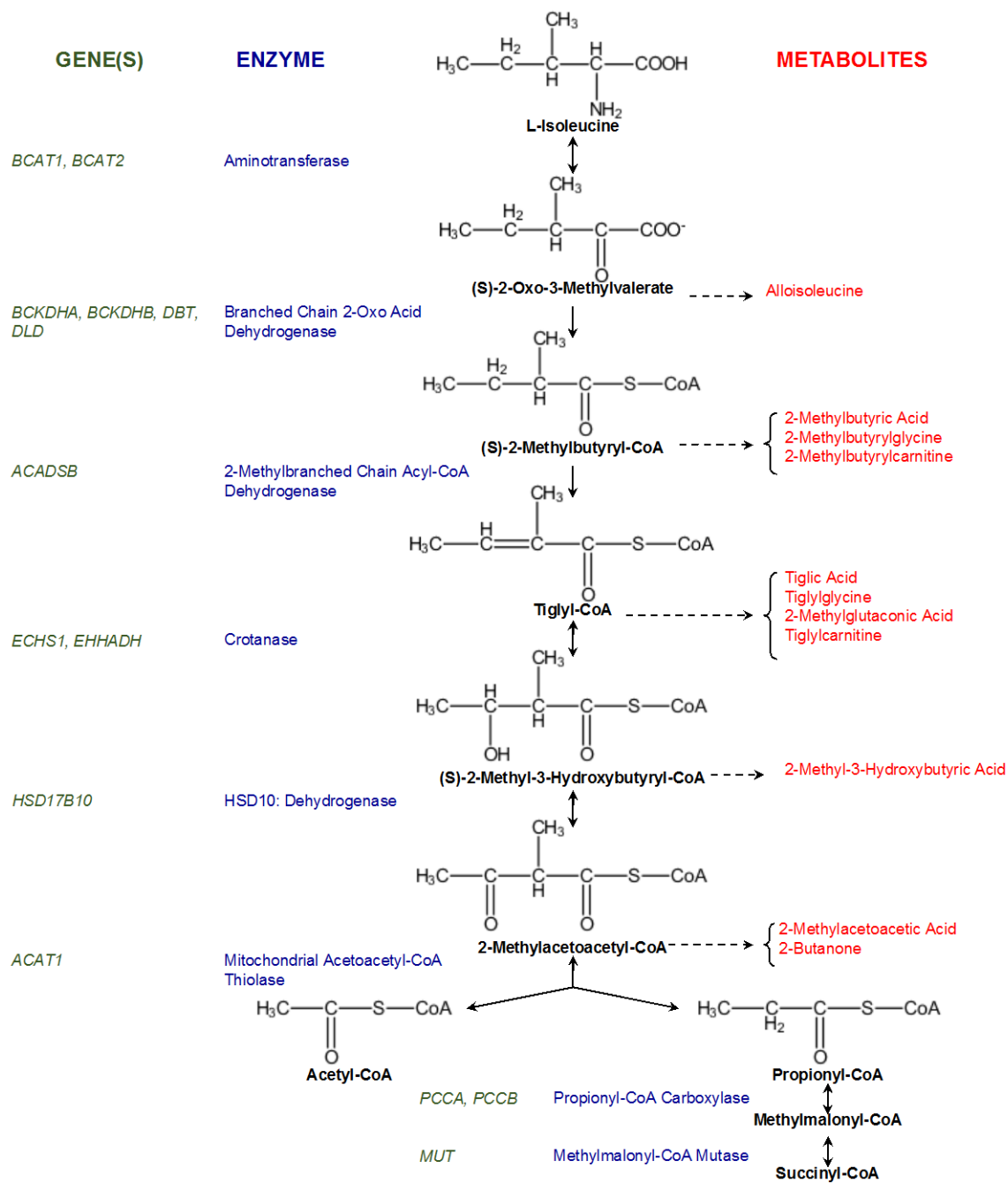
Figure 3. ILE catabolism.

Enzymes involved in ILE catabolism are listed in blue and their relative genes are listed in green (left). Alternate metabolites generated by BCAAs are listed in red (right) at their relative steps in the pathway.
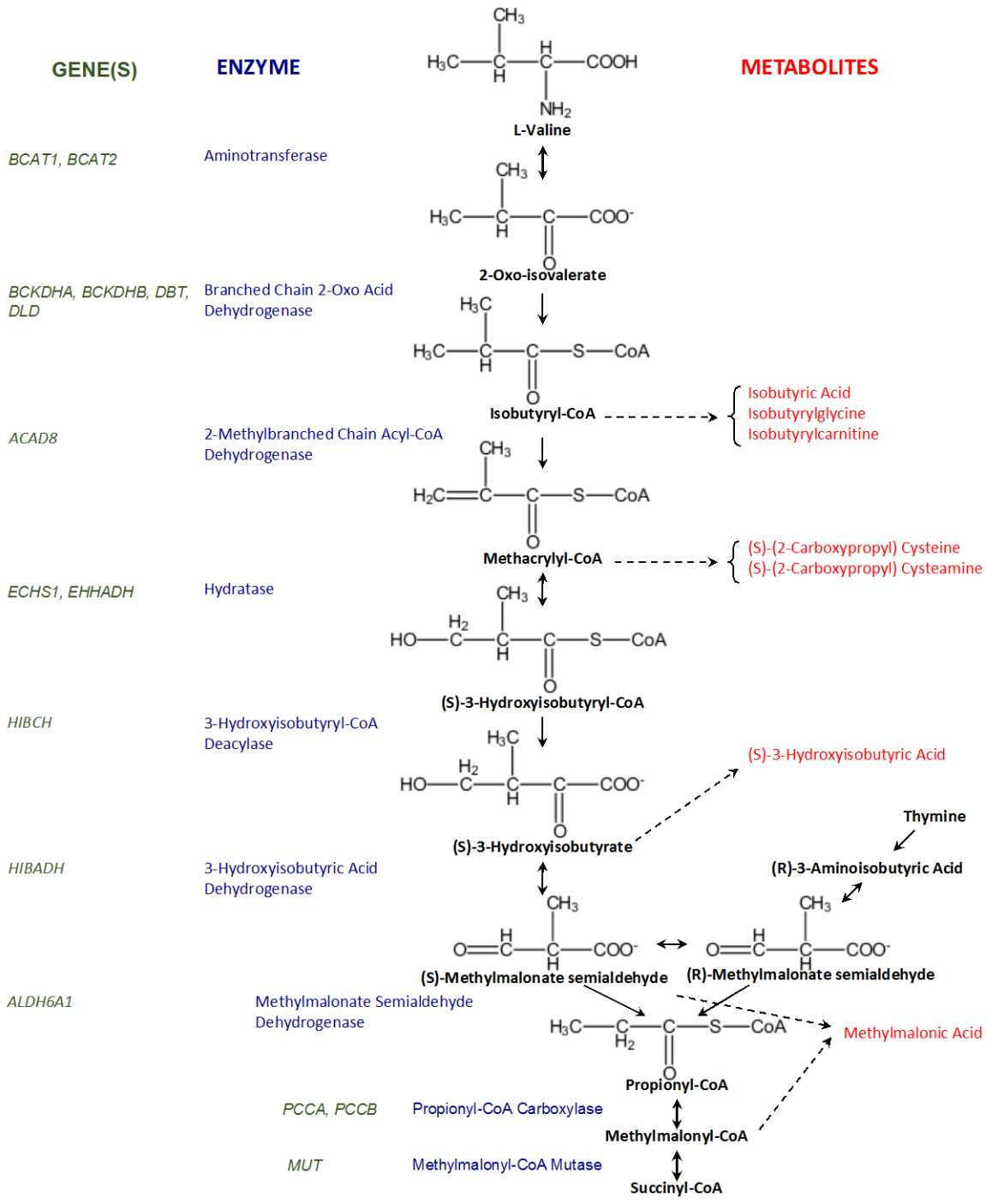
Figure 4. VAL catabolism.

Enzymes involved in VAL catabolism are listed in blue and their relative genes are listed in green (left). Alternate metabolites generated by BCAAs are listed in red (right) at their relative steps in the pathway.

1.1.1 The BCKDH complex

Deficiency of the second shared step of BCAA metabolism, the BCKDH complex, is among the most common disorders of the BCAA catabolic pathway, known as maple syrup urine disease (MSUD)[15,16]. MSUD results in an increased level of BCAAs as well as the accumulation of branched-chain alpha-ketoacids in the plasma and urine–with leucine derivatives being the highest–causing a pronounced odor of maple syrup. MSUD is an autosomal recessive disorder affecting approximately 1 in 185,000, though it is more common in the Mennonite population. Patients with untreated MSUD are at risk for sudden death due to recurrent metabolic crisis and subsequent cerebral edema caused by high levels of leucine in the brain. The BCKDH complex is a 4,000 kDa multimeric enzyme consisting of three catalytic domains: a thiamine pyrophosphate-dependent carboxylase (known as E1), encoded by two genes–*BCKDHA* and *BCKDHB* encoding the α and β subunits; a transacylase E2 subunit, encoded by the gene *DBT* which forms the 24-subunit core of the enzyme; and a dehydrogenase E3 subunit, encoded by *DLD*[15]. BCKDH activity is regulated by a specific kinase and phosphatase through a reversible phosphorylation/dephosphorylation mechanism.

1.1.2 BCAA ACADs

Inborn errors of metabolism caused by mutations in the BCAA ACADs *IVD*, *ACADSB* (encoding SBCAD), and *ACAD8* (encoding IBD) genes involved in LEU, ILE, and VAL catabolism, respectively, have been extensively described, and are now identified through newborn screening by tandem mass spectrometry (MS/MS) in all babies born in the US[1,2]. The overall structure of these ACADs is a homotetramer, with the subunits arranged as a dimer of

dimers. They have a similar tertiary fold consisting of an N-terminal α-helix domain, a β-sheet domain, and a C-terminal α-helix domain. The catalytic residue is a glutamate in all known ACADs.

Isovaleric acidemia (IVA), caused by a deficiency in IVD, was the first organic acidemia recognized when the odor of sweaty feet that surrounded an infant with episodic encephalopathy was shown to be due to isovaleric acid[17,18]. Early literature on IVA, an autosomal recessive disorder, emphasized two apparent phenotypes. The first was an acute, neonatal presentation with patients becoming symptomatic within the first two weeks of life[17,18,19,20,21,22]. Patients appeared initially well, then developed vomiting and lethargy, progressing to coma. The second group presented with relatively non-specific failure to thrive and/or developmental delay (chronic intermittent presentation). In reality, it is now apparent that patients can fall anywhere on the spectrum of acute to chronic presentation and that there is probably little predictive value to the initial presentation[23,24]. Moreover, with the application of MS/MS in newborn screening, numerous asymptomatic patients with one recurring *IVD* gene mutation have been reported[22].

SBCAD deficiency has been described in a patient with dramatic metabolic decompensation as a newborn and significant neurologic sequela; however, it has since become clear that most (if not all) individuals with this deficiency remain asymptomatic[24,25,26]. A common founder mutation in *ACADSB* has been identified in the Chinese Hmong population[26].

IBD deficiency appears to have risk for clinical symptoms intermediate between the other two disorders and is characterized by high urinary loss of acylcarnitine species predisposing to carnitine deficiency and secondary myopathy and cardiomyopathy[13,27,28,29,30]. While these symptoms have been described in some patients, most identified with IBD deficiency through newborn screening have been well[27,30].

IVD shows high specificity for its substrate of LEU, while SBCAD and IBD seem to be more promiscuous. The K_m values for IVD, IBD and SBCAD have been described for each purified enzyme for their substrates (Table 1). IVD appears to have the lowest K_m of 1.0 µM for isovaleryl-CoA[31]. For practical purposes, the value of the K_m can be interpreted as a value inverse to the affinity of the substrate to the enzyme. IBD and SBCAD's K_ms are 2.6 µM and 2.7 µM for isobutyryl-CoA and 2-methylbutyryl-CoA, respectively[32,33]. Additionally, IVD, IBD, and SBCAD can utilize each other's substrates to a lesser extent[33,34].

Table 1. Comparative Kms of human BCAA ACADs (µM).

	Isovaleryl-CoA	2-methylbutyryl-CoA	Isobutyryl-CoA
IVD	1.0	Not reported	N.D.
SBCAD	N.D.	2.7	130
IBD	N.D.	18	2.6

N.D., not detectable

1.1.3 3MCC

3MCC is the ATP-dependent carboxylase that follows IVD in the leucine pathway. The holoenzyme of this protein is 835 kDa and is composed of 3 heterodimers encoded by *MCCC1* (~85 kDa α subunit) and *MCCC2* (~60 kDa β subunit)[35]. Most patients deficient for 3MCC are asymptomatic, though some do experience acute episodes with vomiting, acidosis, hypoglycemia, hypotonia, and coma with physiologic stress[36]. Patients experiencing these symptoms can be treated with protein restriction and carnitine supplementation. While the likelihood to develop clinical symptoms with a primary deficiency of this protein is low, the proximity of 3MCC to other important enzymes in the BCAA pathway, such as IVD, makes it of

potential interest when evaluating the role of changes in a potential structural metabolic complex in disease and treatment development.

1.1.4 PCC and MUT

At the distal end of the BCAA catabolism pathway lies additional clinically relevant enzymes, propionyl-CoA carboxylase (PCC) and methylmalonyl-CoA mutase (*MUT*). PCC catalyzes the reversible conversion of propionyl-CoA to methylmalonyl-CoA. The PCC holoenzyme is composed of 6 α (*PCCA*) and 6 β (*PCCB*) subunits to create a biotin-dependent dodecamer. A defect in either *PCCA* or *PCCB* causes the autosomal recessive disorder propionic acidemia (PPA).

Following PCC, *MUT* catalyzes the reversible step of methylmalonyl-CoA to the generation of the tricarboxylic acid (TCA) cycle intermediate, succinyl-CoA (Figure 5). *MUT*'s quarternary structure is that of a homodimer. A deficiency in *MUT* causes methylmalonic acidemia (MMA), which shares similar symptoms and severity with PPA. Patients with PPA experience accumulation of intermediate BCAA metabolites and a depletion of anaplerotic agents which can cause hyperammonemia, lethargy, vomiting, and can progress to coma or death[37]. PPA is diagnosed by elevated blood C3 in new born screening by MS/MS; however, patients who present at infancy and are treated early may still develop neurodevelopmental sequalae[38]. PPA is estimated to occur in 1:100,000 – 1:150,000 live births in Western populations. PPA also appears to be more common in certain Chinese populations, Inuit populations of Greenland, Amish populations, and Saudi Arabians. Unfortunately, apart from dramatic dietary restrictions or liver transplantation that provides partial symptomatic relief, there are no effective treatments or cures for PPA[39].
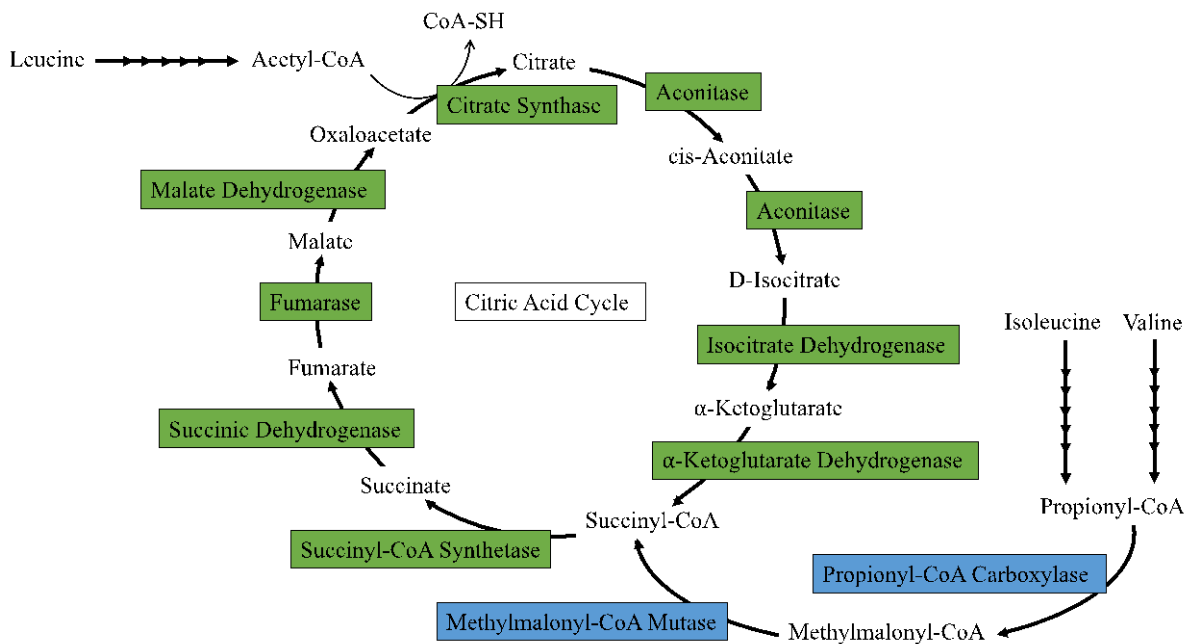
Figure 5. TCA cycle.

Enzymes involved in BCAA metabolism are highlighted in blue boxes. Enzymes of the TCA cycle (also known as citric acid cycle) are in green. Note the usage of LEU, ILE, and VAL as precursors for cofactors or intermediates.

1.2   TREATMENT

1.2.1   Current treatments for BCAA organic acidurias

In all organic acidurias, there are three therapeutic goals. The first is the prevention of metabolic decompensation by careful clinical observation and dietary management. This includes the avoidance of fasting and maintaining anabolism in times of stress (like illness). Reducing the natural protein in the diet for 12-24 hours may help, but additional calories to promote anabolism must be provided. The second goal is long term reduction of the toxic metabolite through

restriction of dietary consumption. Reduction of the toxic metabolite is key for some organic acidurias, such as leucine restriction in IVA, but the proper caloric and amino acid intake to promote normal growth for infants and children must be considered. PPA and MMA patients experience a restriction of an array of amino acids in their dietary consumption: VAL, methionine (MET), ILE, and threonine (THR), due to their ability to generate propionyl-CoA. The individual contributions of the propionyl-CoA progenitors to the cellular propionyl-CoA pool has not been examined.

The third goal for organic aciduria therapuetics is to enhance alternative metabolic pathways to produce non-toxic metabolites that can be readily and safely used or excreted. For example, a common treatment for organic acidurias is the addition of carnitine supplementation to facilitate the removal of intermediate metabolites[40]. However, carnitine supplementation is of minimal therapeutic value. This project, in theory, could have the most profound effect on the second and third goal, as described in the "Hypothesis and Specific Aims" section below. As detailed throughout this dissertation, demonstartion of a promiscuous BCAA metabolon could lead to a new array of potential targets for therapy, while elucidation of the differential contribution to the cellular propioyl-CoA pool could assist in treatment of PPA.

1.2.2   The importance of super-complex discovery in fatty acid oxidation disorders

Previous literature as well as work currently underway in the Vockley lab has identified the existence of a protein super-complex in mitochondria that encompasses the enzymes of fatty acid oxidation (FAO) and oxidative phosphorylation. Historically, enzymes are most often represented as floating free in the cellular milieu, following a "hit and run" method of functionality in which the product of one enzyme is released after the reaction to find the next

enzyme for which it is a substrate. However, the individual respiratory complexes exist in the inner mitochondrial membrane as a super-complex composed of complexes I, III, and IV arranged to promote channeling of electrons, thus increasing catalytic efficiency (Figure 6)[41,42]. Disturbance of the super-complex formation has dramatic clinical effects. For example, a recently published paper shows the effects ACAD9 deficiency has not only on FAO disorders (FAOD) but on mitochondrial dysfunction in general[43]. Some treatments currently in clinical trials involve the use of a cardiolipin binding peptide, elamipretide, to stabilize the inner mitochondrial membrane, and therefore increase cristae folding and stabilize super-complexes[44].

A. "Hit and run" model

B. Stable super-complex formation
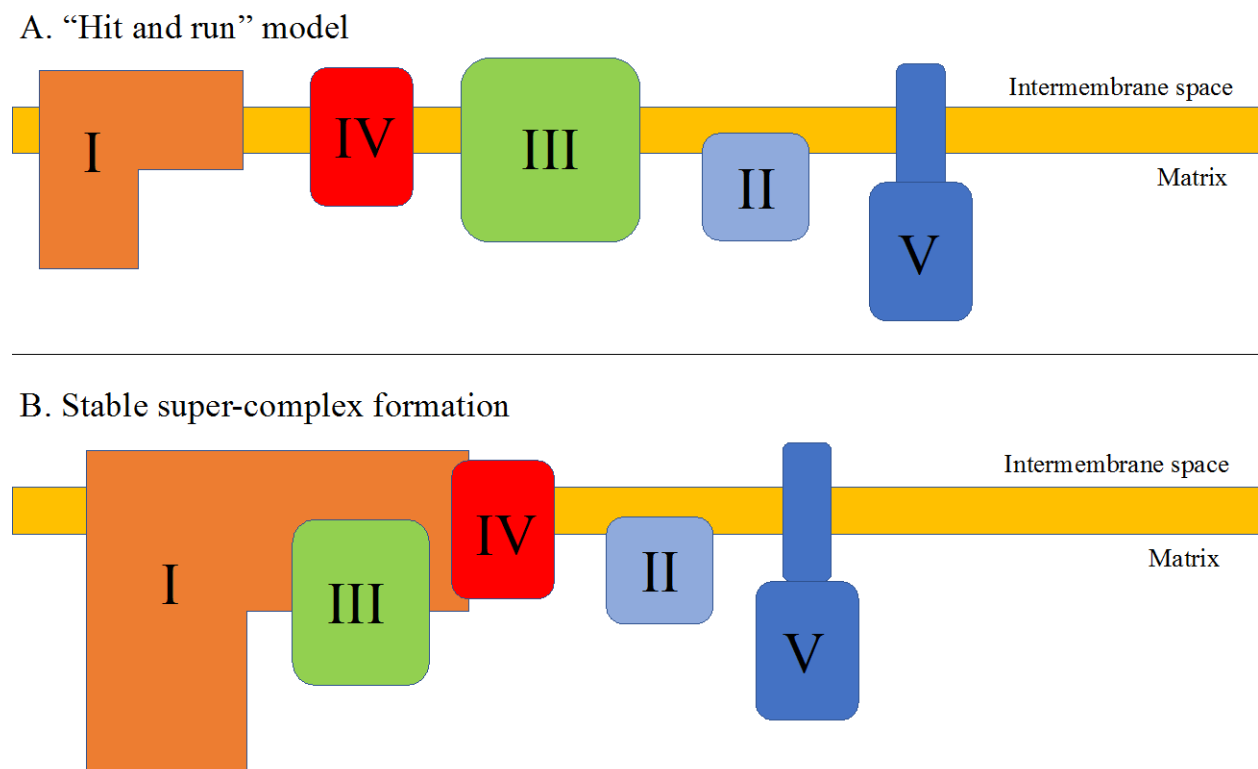
Figure 6. "Hit and run" vs. super-complex models of respiratory chain protein complex architecture.

A. A previous model for respiratory chain complexes in the inner mitochondrial membrane implies the release of substrate into the membrane to be found by subsequent protein complexes. B. The current model of respiratory chain protein complexes organized into a super-complex

allowing smooth transitions of substrate to following enzymes. See text for biological importance. Not to scale.

1.3   PUBLIC HEALTH SIGNIFICANCE

Disorders of branched chain acyl-CoA metabolism are the most common of the organic acidemias identified by newborn screening through MS/MS performed on all babies in the United States[45]. Among these, defects in IVD, SBCAD, and IBD are of great clinical and historical importance. IVA was the first organic academia described[46] and ushered in a new era of metabolic medicine with definition of new diseases through gas chromatography/mass spectrometry. Many of the disorders of BCAA metabolism are now identified through newborn screening and affect ~1:20,000 people combined[45]. Recognition of the benefit of early treatment in prenatally diagnosed babies with IVA played a major role in the adoption of tandem mass spectrometry screening of blood spots from newborn babies for metabolic disease. Newborn screening, in turn, has brought the field full circle, identifying a much broader spectrum of disease than has previously been seen in IVD deficiency, and bringing into question the clinical relevance of IBD and SBCAD deficiency. Better definition of these disorders is critical to intelligent utilization of public health resources in newborn screening, and in the development of appropriate treatment and follow-up schemes for patients.

This project brings together a unique blend of basic science and clinical investigation experience in disorders of the branched chain amino acid catabolism pathways. This project combines metabolomics and proteomic studies to develop an unprecedented understanding of the critical functional interactions necessary for efficient metabolism of branched chain amino acids. These findings will in turn allow a better understanding of the cellular mechanisms that define

clinical risk for individuals with genetic disorders of these enzymes and development of novel therapeutic agents for their treatment.

1.4   HYPOTHESIS AND SPECIFIC AIMS

The goal of this project was to characterize physical and functional interactions between BCAA enzymes and the clinical implications of these relationships for patients with IVA, PPA, and other inborn errors of BCAA metabolism. The physical relationships of the various enzymes in the BCAA pathways are unknown. I hypothesized that the enzymes of LEU, ILE, and VAL catabolism form a functional, yet fluid complex that is distinct from those active in fatty acid oxidation or the respiratory chain (Figure 7). To discover more about overall BCAA metabolism, I examined the metabolic segregation of propionyl-CoA derived from its various precursors. I hypothesized that there would be a differential contribution to the formation of propionyl-CoA from BCAA and odd chain fatty acids, which would provide insights into the development of novel drugs for treatment of these disorders. To directly translate this project from basic science to therapeutics, I tested novel treatments on PPA and MMA patient derived cell lines. Improved therapy may improve the lives and diets of patients with PPA or MMA. The project had three specific aims:

1.4.1 Specific aim 1

1.4.1.1 Specific aim 1a

To employ gel electrophoresis techniques with and without chemical cross-linking to identify interacting partners in the BCAA catabolic pathways. A sensitive and specific MS assay was used to characterize the proteins captured in these experiments. I predicted that BCAA ACADs will interact with the universal BCKDH and with subsequent enzymes, such as 3MCC, in a fluid, yet functional, complex.
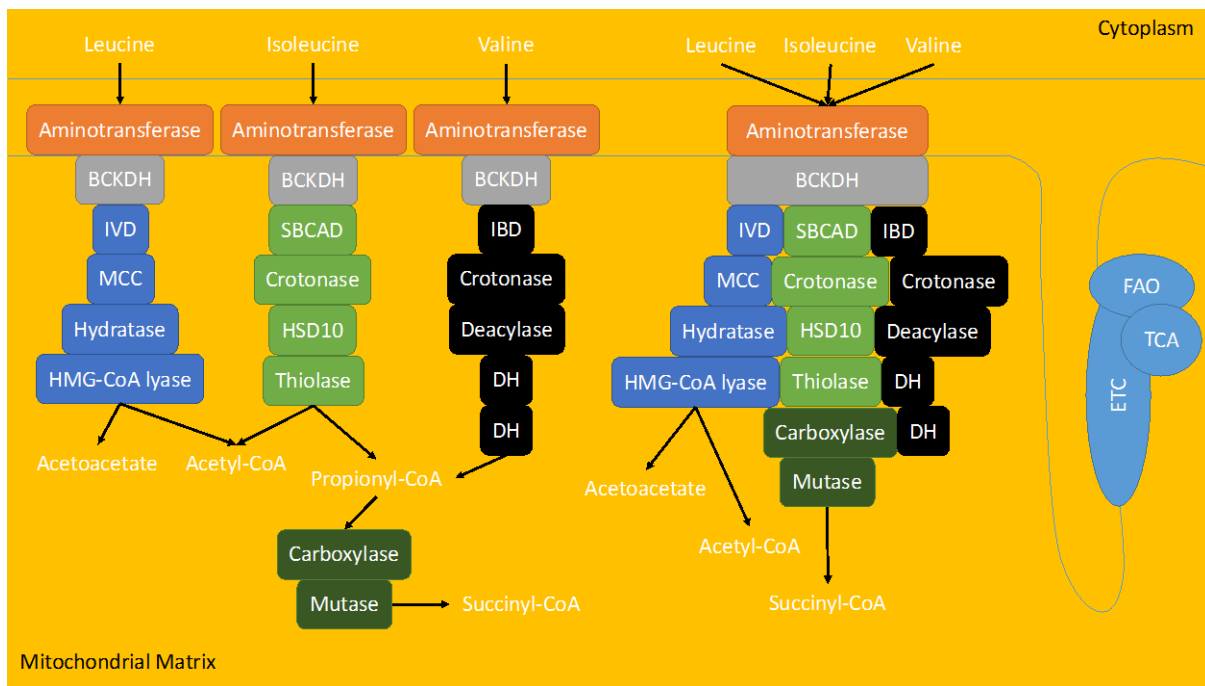
Figure 7. Visual representation of hypothesis.

Here, I am hypothesizing two possible representations of a BCAA super-complex. On the left of the image, I am showing that it is conceivable that the separate pathways of LEU, ILE, and VAL are organized into separate complexes to promote metabolic channeling. On the right, I am showing the possibility that all three BCAA pathway enzymes are organized into a large multifunctional super-complex.

1.4.1.2 Specific Aim 1b

To utilize super resolution microscopy to detect direct contact between BCAA enzymes in cultured cells. Stimulated emission depletion (STED) imaging was utilized to directly examine protein-protein interactions. Control (WT) cells were treated with antibodies specific to a combination of enzymes in the BCAA for fluorescent imaging. Standard confocal imaging allows direct visualization of co-localization at a resolution of 250-300 nm. STED, in contrast, allows a resolution of 60-100 nm to examine co-localization at a much more precise level. I predicted that BCKDH, the ACADs, and 3MCC would all demonstrate a direct interaction, defining a BCAA metabolon.

1.4.2 Specific Aim 2

1.4.2.1 Specific Aim 2a

To characterize metabolic channeling through the BCAA pathways. Previous literature has shown that there is significant substrate sharing, or promiscuity, between the ACADs involved in BCAA metabolism. Metabolism of ILE and VAL by SBCAD and IBD suggest possible interactions of their catabolic pathways with each other and that of LEU. Using universally labeled stable isotopes and patient derived cell lines, I evaluated these interactions. Significant promiscuity of the ACADs and other BCAA proteins would imply geographical proximity of these enzymes within the mitochondria. Geographic proximity can, in turn, indicate a BCAA super-complex, suggesting additional options for patients with BCAA organic acidurias.

1.4.2.2 Specific Aim 2b

To demonstrate differential contributions to the propionyl-CoA pool derived from stable isotope labeled branched chain amino acid and odd chain carbon fatty acid substrates. Metabolic flux studies performed in collaboration with Agios Pharmaceuticals were used to examine the amounts of propionyl-CoA derived from ILE and VAL compared to that derived from heptanoate and other amino acids of interest. These studies will impact proposed anaplerotic therapies for FAODs and BCAA metabolism currently underway.

1.4.3   Specific Aim 3

To apply novel therapeutics to PPA and MMA cell lines. Patient derived fibroblast cells lines were grown in culture and treated with two different molecules. The first was succinate, an anaplerotic treatment, or a substrate that can enter the TCA cycle directly to replenish the metabolic blocks in disorders like PPA and MMA. I predicted that succinate would ameliorate a TCA deficit caused by PPA and MMA. The second treatment was a cardiolipin binding peptide, similar to elamipretide. Cardiolipin is a mitochondrial specific phospholipid molecule that, due to its shape, allows formation of the cristae by the inner mitochondrial membrane[47,48]. When oxidized in disorders of energy metabolism, mitochondria become less stable and energy metabolism is adversely affected. Stabilization of the inner membrane structure by the addition of the cardiolipin binding peptide, has been shown to increase respiratory chain super-complex formation and function. I predicted that treatment of PPA or MMA cell lines with a novel cardiolipin binding peptide would improve cellular bioenergetics. The two mentioned treatments were tested by Western blotting to measure protein abundance; MitoSox to measure ROS reduction; and MitoTracker to measure mitochondrial mass reduction.

2.0   PROTEOMICS AND IMAGING DEFINES A NOVEL BCAA SUPER-COMPLEX

2.1   MATERIALS AND METHODS

Materials

Rat liver mitochondria – 8.2 mg/mL; see preparation below

PBS
– 160 g NaCl + 4 g KCl + 28.4 g Na_2HPO_4 + 4.8 g KH_2PO_4 + 1L H_2O = 20X stock; 50 mL 20X PBS stock + 950 mL H_2O = 1 L 1X PBS

HB buffer
– 4 mL 0.5M EDTA + 50 mL glycerol + 6 mL 1 M KH_2PO_4 + 94 mL 1 M K_2HPO_4 + 171.15 g sucrose + 2 L H_2O

HEPES
– 30 mM HEPES free acid (OmniPur; Cat#5320) + 150 mM potassium acetate; in H_2O

Cross-linkers
  BM(PEG)₃
– 1,11-bis(maleimido)triethylene glycol;
– Thermo Scientific; Cat#22337;
– 17.8 Å hydrophilic; homobifunctional, maleimide for conjugation between sulfhydryl groups

  EGS
– ethylene glycolbis(succinimidylsuccinate)
– Thermo Scientific; Cat#21565;
– 16.1 Å hydrophobic; homobifunctional *N*-hydroxysuccinimide (NHS) ester

  LCSMCC
–Succinimidyl-4-(N-maleimidomethyl)cyclohexane-1-carboxy-(6-amidocaproate)
– Thermo Scientific; Cat#22362;
– 16.2 Å, hydrophobic; heterobifunctional NHS ester and maleimide groups allowing conjugation of amine- and sulfhydryl-containing molecules

Sulfo-EGS	– ethylene glycolbis(sulfosuccinimidylsuccinate); – Thermo Scientific; Cat#21566; – 16.1 Å hydrophilic; homobifunctional *N*-hydroxysuccinimide ester
PBST	– 1 L 1X PBS + 1 mL Tween20 (Sigma; Cat#P7949)
Coomassie stain	– 0.1% R_{250} (BioRad; Cat#161-0400) + 7% acetic acid + 40% MeOH + 42.9% H_2O
Coomassie de-stain	– 10% acetic acid + 40% MeOH + 50% H_2O
Digitonin	– MilliPore; Cat#300410; 1/5 ratio of sample/digitonin suspended in HEPES to create 4mg/mL
Complete media	– 500 mL Dulbecco's modification of Eagle's media (DMEM) (Corning; Cat#10-013-CV) + 50 mL fetal bovine serum (FBS) + 5 mL L-glutamine + 5 mL penicillin/streptomycin
Trypsin	– Corning; Cat#25-053-CI
PBB	– PBS + 2% bovine serum albumin (BSA); 2.0 g BSA + 100 mL PBS

Mitochondrial isolation from rat liver

Rat liver was extracted from sacrificed rats. The liver was then sheared into ~1 cm^3 pieces and washed multiple times with ice cold PBS until blood was washed out. All PBS was drained, and sheared livers were suspended in HB buffer containing 1 mL protease inhibitor/20 g tissue. Samples were then finely sheared on ice using an electric homogenizer in 30 s intervals with a 5 min rest on ice in between shearing. Samples were then centrifuged at 4,000 rpm for 5 min. The supernatant was transferred to another vial to centrifuge at 14,000 rpm for 15 min. The supernatant was discarded. Finally, the outer, light-colored pellet containing the mitochondria was suspended with 1 mL of HB buffer. Samples were frozen at -80 ºC for future use. Protein concentration was calculated via DC BioRad protein concentration assay according to the manufacturer's instructions.

Cross-linking and sample prep

0.5 mL rat liver mitochondria were taken and suspended in 300 µL HEPES buffer. The samples were then incubated with the following cross-linkers in incremental amounts:

Table 2. Cross-linker testing grid of incremental concentrations.

Final mM LCSMCC	0 mM	0.4 mM	2 mM	4 mM
Volume µL from 10mM LCSMCC	0 µL	12 µL	60 µL	120 µL
Final mM BM(PEG)$_3$	0 mM	0.2 mM	2 mM	4 mM
Volume µL from 20mM BM(PEG)$_3$	0 µL	3 µL	30 µL	60 µL

Cross-linkers and samples were incubated for 40 min in room temperature (RT), as per manufacturer's instructions. After incubation, 15 µL of 1 M Tris-HCl pH 7.1 were added and incubated for 15 min at RT to stop cross-linking reaction. Samples were then combined with equal amounts of 2X Laemmli SDS buffer (Sigma; Cat#S3401) for 5 min at 95 ºC. Samples were loaded into 4-15% gradient criterion SDS gel (BioRad; Cat#3450027) with pattern below:

Table 3. General loading pattern for SDS-PAGE.

Well	Description	Amount	Purpose
1	Molecular marker (BioRad; Cat#161-0374)	5 µL	Western
2	Control	30 µL	
3	<1mM BM(PEG)$_3$		
4	2mM BM(PEG)$_3$		
5	4mM BM(PEG)$_3$		
6	<1mM LCSMCC		
7	2mM LCSMCC		
8	4mM LCSMCC		
9	Pure IVD	3 µL	
10	Molecular marker	5 µL	Staining
11	Control	30 µL	
12	<1mM BM(PEG)$_3$		
13	2mM BM(PEG)$_3$		
14	4mM BM(PEG)$_3$		
15	<1mM LCSMCC		
16	2mM LCSMCC		
17	4mM LCSMCC		
18	Pure IVD	3 µL	

Western blotting

The gel was run for 2 hrs at RT and 80V constant. The gel was transferred to a PVDF membrane for 35 min at 0.3 A constant. The western membrane was blocked overnight in 10% dry milk in PBST at 4 ºC or for 40 min at RT, washed briefly with PBST, and then twice again with PBST for 5 min each at RT. The membrane was then incubated with a dilution of 1:300 primary antibody in 1% milk in PBST for 1 hr at RT or overnight at 4 ºC. Commercial antibodies were used according to manufacturer's instructions/suggestions. The membrane was washed 3X with PBST for 5 min each at RT, incubated with a dilution of 1:2000 goat-anti-rabbit/mouse HRP conjugate (BioRad; Cat#170-6515) secondary antibody in 1% milk protein in PBST for 1 hr at RT. The membrane was washed 3X with PBST for 5 min each, then incubated with 3 mL Pierce ECL western blot substrate (Thermo Scientific; Cat#32106) without prior mixing. Finally, the

membrane was briefly dried for 5 min in a fume hood. X-ray film was placed on membrane in dark room for 1 – 5 min, or as needed to obtain clear picture after development.

Table 4. Antibodies used for Western blotting.

Antigen	Source	Dilution	Clonality
BCKDHB	Mouse	1:200	Monoclonal
IBD	Mouse	1:100	Monoclonal
IVD	Rabbit	1:300	Polyclonal
MCCC2	Rabbit	1:200	Polyclonal
MUT	Mouse	1:100	Monoclonal
VDAC1	Mouse	1:100	Monoclonal

Whole protein stain

The gel was placed in staining solution containing R_{250} for no more than 30 min. Gel was then de-stained for 30 min. The de-stain was removed, replaced, and de-stained for another hour. If banding patterns remained unclear, the de-stain was removed and replaced once again and left to de-stain overnight at RT. For best imaging quality, the gel was left to rehydrate in water overnight at RT.

Proteomic analysis

Bands of interest were identified from western blots and cut from the de-stained gel and sent to the University of Pittsburgh MS Proteomics Core Facility. An in-gel reduction alkylation trypsin digestion was applied to samples and the extracted tryptic peptides were analyzed using liquid chromatography tandem mass spectrometry (LC-MS/MS) followed by database searching to obtain amino acid sequence[49,50,51].

2D gel electrophoresis

For a two-dimensional gel, first a blue native-PAGE (BNGE) protocol was run. To begin BNGE, rat liver mitochondria samples were prepared as above and centrifuged at 5,000 rpm for 10 min. While centrifugation was taking place, a digitonin/HEPES master mix was made and incubated at 95 ^{o}C for 5 min to dissolve solution. The digitonin mixture was placed on ice for at least 20 min. The master solution was added to the samples to give a 1/5 ratio of protein/digitonin and a 4 mg/mL protein concentration. The samples were incubated on ice for an additional 30 min. Coomassie blue stain was added to samples at a 1:20 – 1:30 dilution and re-suspended by pipette. Samples were centrifuged at 17,000 rpm for 1 hr at 4 ^{o}C. Supernatants were transferred to new vials carefully so as to not disturb the pellets. Pellets were discarded. Samples were stored in -80 ^{o}C until used. Samples were loaded onto a 3-12%, 10-well bis-tris gel (Native-PAGE; Thermo Scientific; Cat#BN1001BOX). The gel was run at 80 V constant for 4-5 hrs at 4 ^{o}C, then stained with R$_{250}$ Coomassie stain for 15 min, and de-stained for 30 min, 1 hr, or overnight at RT when necessary as described above.

When the Native-PAGE gel was fully de-stained, the lanes were cut and submerged in 2X Laemmli buffer for 1 hr in RT in a fume hood. The lanes were then washed with tris/glycine/SDS gel running buffer (National Diagnostics; Cat#EC-870) until the buffer read a pH of 7 (usually about 5 min washes). In order for the gel strips to be placed on a Prep-+2 SDS-PAGE gel, they were briefly dried under in a fume hood for 5 min. The gel strips were carefully placed into the large well of the Prep-+2 SDS-PAGE gel and the gel was run as above at 80 V constant for approximately 2 hr. The gel was transferred to a membrane, and the membrane stained with appropriate antibodies as indicated in the results.

Immunofluorescence

Control, wild-type, patient derived fibroblast, or HEPG2 cells were grown in culture with complete media changed every 48 hrs. Fibroblast cells are isolated from an 8-year-old male with a passage of 2-10. Cells were grown to 90% confluence and seeded onto coverslips by trypsinzation. To trypsinize cells in a T175 flask: the media was removed, the flask of cells was washed with 10 mL PBS, and ~2.5 mL trypsin was added for 5 min in 37 $^{\circ}$C/5.0% CO_2. 10 mL DMEM was then added to stop reaction of trypsin. Viable cells were counted by saving 1 mL of cells/trypsin/media and by using a Beckman Coulter Life Sciences Vi-Cell counter. Slide coverslips were exposed to UV light for at least 15 min, placed into a 12-well plate, coated with poly-L-lysine for 5 min at RT, and allowed to dry under a class II type A2 biosafety cabinet for an additional 15 min. The cells were seeded at approximately 50,000 viable cells/well to generate a monolayer and grown overnight at 37 $^{\circ}$C with 5.0% CO_2. The media was removed, and 3 brief washes of PBS followed. The cells were fixed using 2% paraformaldehyde in PBS for 15 min at RT and washed 2X in PBS. Samples were then stored in 4 $^{\circ}$C for a maximum 6 months submerged in PBS. Otherwise, the cells were permeabilized with 0.1% Triton x-100 made in PBS for 15 min. The samples were washed 3X with PBS, followed by 5X washes with PBB. The samples were blocked using 5% donkey serum albumin (DSA) in PBB for 45 min at RT then washed 5X with PBB. For the primary antibodies solution, commercial antibodies were diluted to 2 µg/mL in PBB. Two antibodies could be added to the same solution provided they were from different host species (i.e. rabbit and mouse). Before applying primary antibodies to the cells, solution was vortexed, centrifuged at 10-12K rpm for 5 min, and only the solution from the top of the vial was used. The coverslips were incubated for 1 hr at RT or overnight at 4 $^{\circ}$C. Again, cells were washed 5X with PBB. For the secondary antibodies solution, AlexaFluor 555

and 647 were diluted 1:2000 in in PBB. From this step forward, efforts were made to keep antibody solutions and samples in dark conditions. Antibody dilution was vortexed, centrifuged at 10-12K rpm for 5 min, and the bottom of the vial was avoided. The secondary antibodies were added in tandem. The cells were incubated for 1 hr at RT, washed 5X with PBB followed by 5X washes with PBS, the stained with DAPI (life Technologies; Cat#1802093) adding 2 drops/mL of PBS to the monolayers. Coverslips were incubated for 5 min at RT with the DAPI stain, then washed 3X with PBS. Finally, coverslips were mounted on clean microscope slides with Prolong Diamond (Thermo Scientific; Cat#1858790) with the cells facing down, avoiding any air bubbles. Fluorophores are brightest and therefore highest quality after 5 days after exposure to Prolong Diamond and are stable up to 3 months in 4 ºC.

Table 5. Antibodies used for imaging.

Antigen	Source	Dilution	Clonality
VLCAD	Mouse	1:50	Monoclonal
HADHA	Rabbit	1:500	Monoclonal
IVD	Mouse	1:100	Monoclonal
MCCC2	Rabbit	2 μg/mL	Polyclonal
ACADSB	Rabbit	2 μg/mL	Polyclonal
ATP5B	Mouse	1:50	Monoclonal
TOM20	Rabbit	2 μg/mL	Polyclonal

STED imaging

STED imaging was carried out in collaboration with the University of Pittsburgh Center for Biological Imaging (CBI). In brief, STED imaging works by simultaneously exciting a particular fluorophore and dampening the surrounding signal with incident photons[52,53,54]. To achieve the large number of incident photons to selectively deplete the surrounding signal, a high intensity laser must be used. This has positive and negative effects. The higher intensity laser forces the

photons to relax at a higher vibrational state, meaning the original emission (as seen in traditional confocal microscopy) can effectively be ignored giving a cleaner signal. However, the high intensity lasers can lead to photobleaching, which can be minimized by increasing antibody concentration and therefore fluorescent signal. As opposed to other super-resolution microscopy (such as FRET), STED lasers will excited two separate fluorophores for direct imaging of protein-protein co-localization at a resolution of 60-100 nm. To put this in perspective, confocal imaging will consistently show co-localization with confidence at a resolution of 250-300 nm. As a baseline for mitochondrial imaging, FAO enzymes known by the Vockley lab to co-localize were imaged first in fibroblast cells.

2.2 SPECIFIC AIM 1: RESULTS

2.2.1 BCAA enzymes co-migrate on a denaturing gel

To examine the physical relationships of the enzymes of BCAA metabolism, rat liver mitochondria were isolated and incubated with various types and concentrations of cross-linking agents (see methods for details on cross-linkers used). Treated samples were run on SDS-PAGE gels for approximately 2 hr at 80 V constant power. The gels were then transferred to a PVDF membrane for western blot analysis. The western blots were performed using a variety of monoclonal and polyclonal antibodies against BCAA metabolism protein subunits from commercial resources to stain the membranes. After many iterations of this process with different cross-linkers and antibodies, a consistent pattern emerged. Figure 8 shows a few representative examples of these experiments. In these gels, the red arrows identify consistently

seen immunoreactive bands at a higher molecular mass than expected for each protein were it migrating separately from other proteins. These high molecular mass bands were only present in cross-linked conditions, and they increased in intensity as the concentration of the cross-linking increased as seen in the MCCC2 Western blot in Figure 8. The consistent bands were located just above the 250 kDa molecular weight marker (hereafter referred to as the ~300 kDa band). This band migrates at a position that is too large to be the monomer of any of enzymes to which the antisera used in the experiment was raised. A second consistent band appeared at a position just entering the gel (hereafter referred to as the >500 kDa band). It also was only present in cross-linking conditions. This band must represent a protein complex so large that it does not readily enter the denaturing SDS gel. Meanwhile, the monomer ACAD size of ~40 kDa was visible in all lanes with varying cross-linker concentration. In the IVD blot seen in Figure 8, as an example, several findings are notable. The control lane contains bands at 40, 80, and 160 kDa, representing the monomer, dimer, and holoenzyme of a typical BCAA ACAD. As there was also a significant amount of background signal on the blot, the higher molecular mass bands (~300 and 500 kDa) were excised and analyzed by mass spectrometry analysis at the University of Pittsburgh Mass Spectrometry core facility in order to unequivocally identify the presence of IVD or other BCAA proteins. Proteins in the BCAA metabolic pathway were catalogued as described for Figure 10.
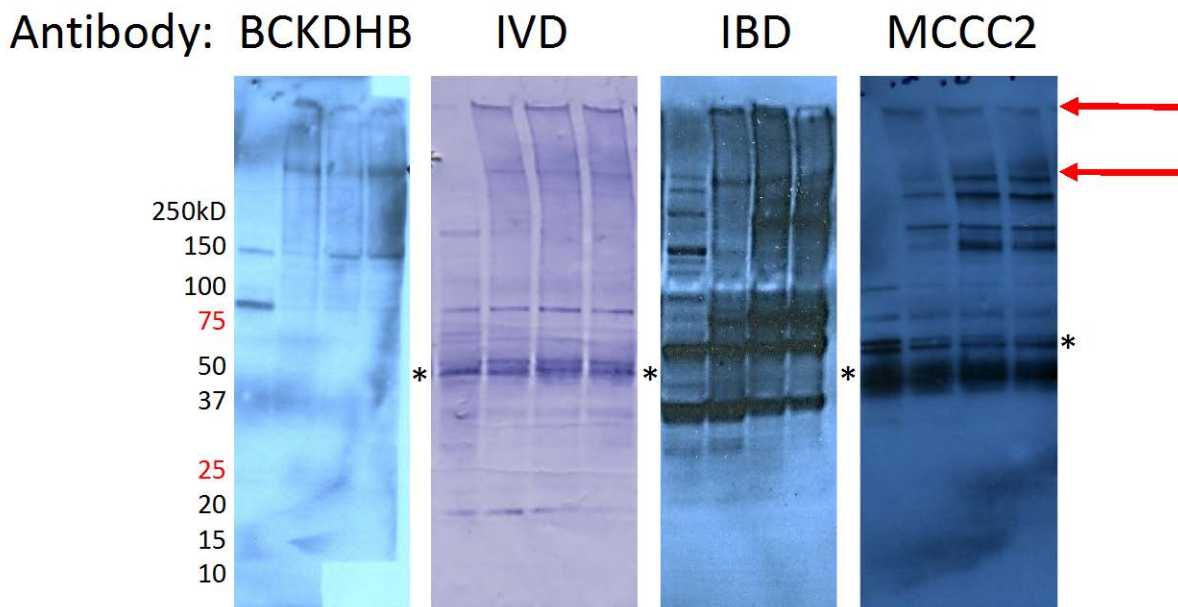
Figure 8. Western blotting results.

Extracts of BM(PEG)$_3$ cross-linked liver mitochondria were separated on SDS-PAGE gels, transferred to nitrocellulose membranes, and visualized with antibodies as listed at the top of each gel section. The red arrows to the right identify bands that were consistent across multiple repetition of gels. The migration of BioRad Precision Plus Dual Color Protein Standard molecular mass markers is shown to the left of the gel. The enzyme monomer size is shown by an asterisk to the right of each membrane. Upper and lower limits of cross-linker concentration are defined by the manufacturer as 0.2 mM – 4 mM.

In these experiments, rat liver mitochondria were isolated, treated with an 18 Å cross-linker which showed the clearest and most consistent banding in the ~300 kDa and >500 kDa region of the gels. A non-cross-linked purified IVD was run alongside the gel as a control. The samples were separated by SDS-PAGE, the gel was stained with Coomassie blue to visualize all proteins, and bands from the gel were excised as shown in Figure 9 for analysis by mass spectrometry. Figure 10 shows the proteins identified. Though Figure 10 shows BCAA protein subunits only, the exhaustive list of proteins identified by MS is available upon request.
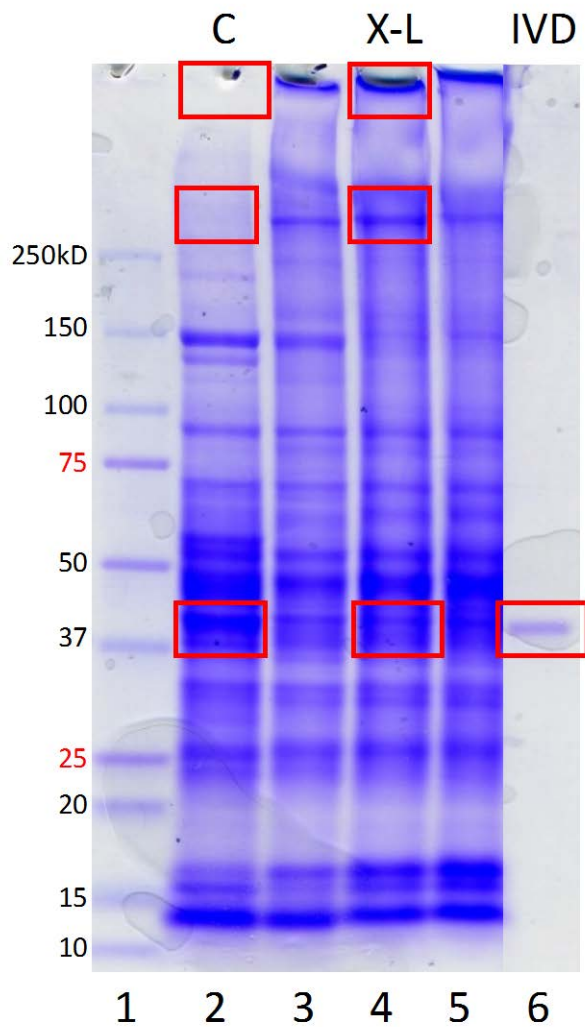
Figure 9. Whole protein stain of SDS-PAGE gel.

The samples loaded were C = control; X-L = cross-link; IVD = purified IVD. The lower and upper limits of the cross-linker were defined by manufacturer's instructions as 0, 0.2 mM, 2 mM, and 4 mM BM(PEG)$_3$ in lanes 2-5, respectively. The ~300 kDa band, >500 kDa band, and the 40 kDa band, shown in a red box were excised and analyzed by mass spectrometry. Molecular mass markers are listed on the left.

Figure 1 No.	BCAA Gene	>500kDa		~300kDa		40kDa		
		Control	Cross-linked	Control	Cross-linked	Control	Cross-linked	Pure IVD
0	BCKDHA	0	0.81008	0	0.78221	3.358	3.5524	0
	BCKDHB	0	4.8605	0	1.5644	3.358	0.71048	0
	DBT	0	1.6202	0	0.78221	0	0	0
	DLD	0	1.6202	0	0.78221	0	0	0
1	IVD	0	1.6202	0	1.5644	15.671	7.8153	72.992
2	ACADSB	0	0	0	0	6.716	0	0
4	MCCC2	0	0	0	3.911	0	0	0
5 6	ECHS1	0	2.4302	0	0	0	0	0
	EHHADH	0	17.822	6.1583	13.298	5.037	0	0
9	HIBCH	0	0	0	0	3.358	0.71048	0
11	ACAT1	0	2.4302	0	0.78221	16.23	10.657	0
12	HIBADH	0	4.8605	0	1.5644	0	0	0
13	ALDH6A1	4.5322	9.721	0	5.4755	2.7983	1.421	0
14	PCCA	0	1.6202	0	0.78221	0	0	0
	PCCB	0	2.4302	0	2.3466	0	0	0

Scale: 0 ————————————————— 20+

Figure 10. Heat map of BCAA mitochondrial proteins identified in gel slices by MS.

The quantities in each cell of this map represent the quantitative value of each protein normalized to the entire spectra, as provided by the MS facility. The individual quantities from each gel slice isolated in Figure 9 are shown. The key at the bottom of the figure shows that darker green represents higher spectral counts of BCAA protein subunit found in each band; a quantitative value of 0.1 – 4.0 is shown in the palest green, while a quantitative value of 20+ is shown in the darkest green. Cross-linked gel slices show a much higher abundance of BCAA protein subunits than their non-cross-linked counterparts. Pure IVD was run alongside the gel from Figure 9 and analyzed via MS as a control.

The mass spectrometry results clearly show a difference between control rat liver mitochondria versus cross-linked rat liver mitochondria. The >500 kDa and ~300 kDa bands contain a significant number of BCAA proteins in the cross-link samples, but not from control. In contrast, BCAA proteins appears in both control and cross-link lanes in the 40 kDa "monomer-sized" band but with much different quantities. Thus, cross-linking of mitochondria prior to separation leads to their migration in higher molecular mass positions on the gel. As seen in Figure 10, there is dramatic prevalence of BCAA subunits in the higher molecular weight bands in cross-linked vs control mitochondria. These results are consistent with the presence of

high molecular mass protein complexes in mitochondria that contain multiple proteins involved in BCAA metabolism, suggesting that these proteins form a metabolon that promotes metabolic channeling. Still, we are unable to determine which proteins are binding to which. IVD, for example, at ~300 kDa must represent more than the holoenzyme by itself. The ~300 kDa band could represent the IVD holoenzyme plus a binding partner, but this partner is not likely MCCC2 as MCCC2 forms a stable hexamer of ~300 kDa by itself. It is more likely that IVD is binding to members of the BCKDH complex (BCKDHA, BCKDHB, DBT, or DLD) at the ~300 kDa band and the presence of MCCC2 in the ~300 kDa band is due to its own hexamer formation. The >500 kDa band could represent the BCKDH complex, IVD, and MCCC, but it remains unclear by MS identification alone if these proteins are cross-linking to one another.

2.2.2   Enzymes of the LEU pathway co-migrate in two-dimensional gel analysis

Next, 2-dimensional (2D) gel electrophoresis was performed with rat liver mitochondria prepared with and without cross-linker. The cross-linker EGS was used in this experiment due to its ability to be chemically cleaved and restore the individual molecular masses of proteins. Digitonin treated samples were first separated in a non-denaturing gel in cold conditions for 4.5 hrs at 80 V constant. The gel was then stained with Coomassie blue, and the gel lanes were excised and submerged in Laemmli buffer. Finally, the gel lanes were washed, placed horizontally in a denaturing SDS-PAGE gel, and run for second dimension separation. The SDS-PAGE gels were then transferred to a PVDF membrane and stained with antibodies to the first three enzymes of the LEU pathway. Results are shown in Figure 11. Here, it is clear that the Western blot identifies BCAA metabolic proteins in higher molecular mass forms than expected for isolated proteins. This high molecular mass form is apparent only in cross-linked sections of

the 2D gels. Superimposition of the three gels demonstrates that BCKDHB, IVD, and MCCC2 are all contained in nearly identical positions in higher molecular mass regions of the native gel. These positions are well above the molecular mass of the individual proteins when mitochondria are treated with a cross-linking agent. These results are again consistent with the presence of a macromolecular complex in mitochondria containing multiple BCAA metabolic proteins.
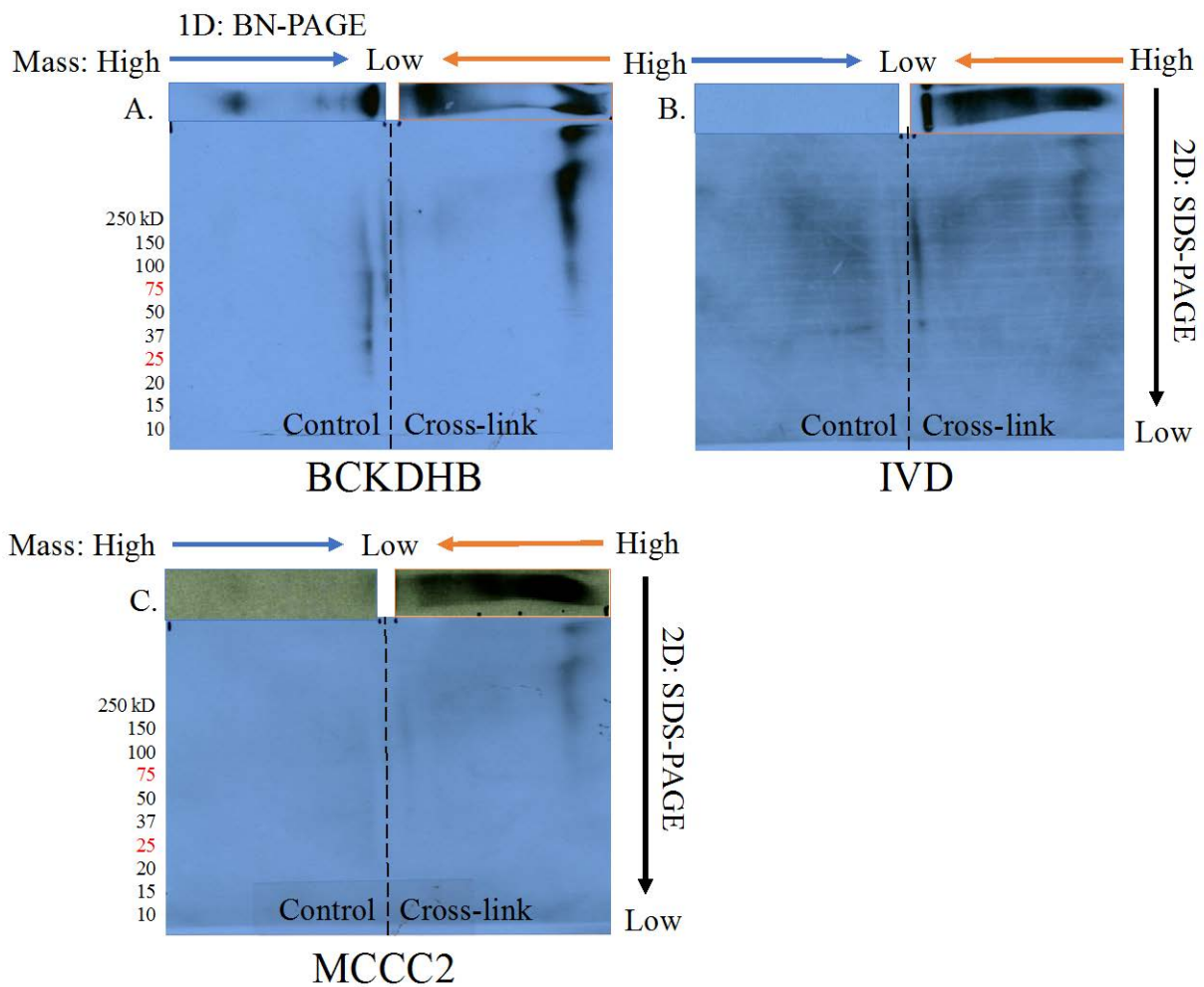
Figure 11. 2D results.

Gel slices from the native gel (first dimension) are shown across the top of the second dimension. The top of the gel, or the higher molecular weight in the first dimension is located on the far left and far right of the 2D blot as indicated by the arrows at the top of the blots. Note also that the native gel slices were cut off at 5 cm to fit in the 2D SDS gel, resulting in little or no

stain in the control sections of the Western blots. The center of the gel is marked with a dashed black line.

2.2.3 Direct Imaging of LEU pathway proteins using STED confirms new model of BCAA super-complex

To characterize directly the potential interactions of BCAA metabolic enzymes, imaging experiments of fibroblast cells were performed using confocal and STED microscopy. Wild type fibroblast cell lines were grown to confluence in T175 flasks, seeded onto glass cover slides as a monolayer, and fixed after 24 hrs for analysis. The slides were incubated with primary antibodies of two proteins produced in different species. For example, a mouse and a rabbit antibody were used in tandem. Next, the cells were treated with secondary antibodies specific for each primary antibody conjugated to fluorophores AlexaFluor 555 and AlexaFluor 647. Confocal and STED images were captured with the assistance of the University of Pittsburgh's Center for Biological Imaging. As a positive control, antibodies to fatty acid oxidation proteins were first used, previously shown by the Vockley lab to directly interact with each other and the respiratory chain, forming a multifunctional super-complex within the mitochondria. Figure 12 shows, confocal microscopy of cells stained with antibodies to the HADHA protein, the alpha subunit of the mitochondrial fatty acid oxidation trifunctional protein (shown in red), and VLCAD antibodies, an ACAD responsible for catalyzing the first intra-mitochondrial step of fatty acid oxidation for long chain substrates (shown in green). The two proteins are seen to co-localize (yellow in merged images). While confocal microscopy demonstrates localization in subcellular compartments, its resolution is only ~200 nm at its best. In contrast, STED technology captures images with a pixel size of 20 nm, implying co-localization at a level of ~60 nm. To put this in

perspective, a typical mitochondrion is approximately 1-2 μm in diameter. Another method of super-resolution microscopy, Forster resonance energy transfer (FRET), will show co-localization of 8-10 nm; however, this technique yields a higher rate of false negative results than STED.
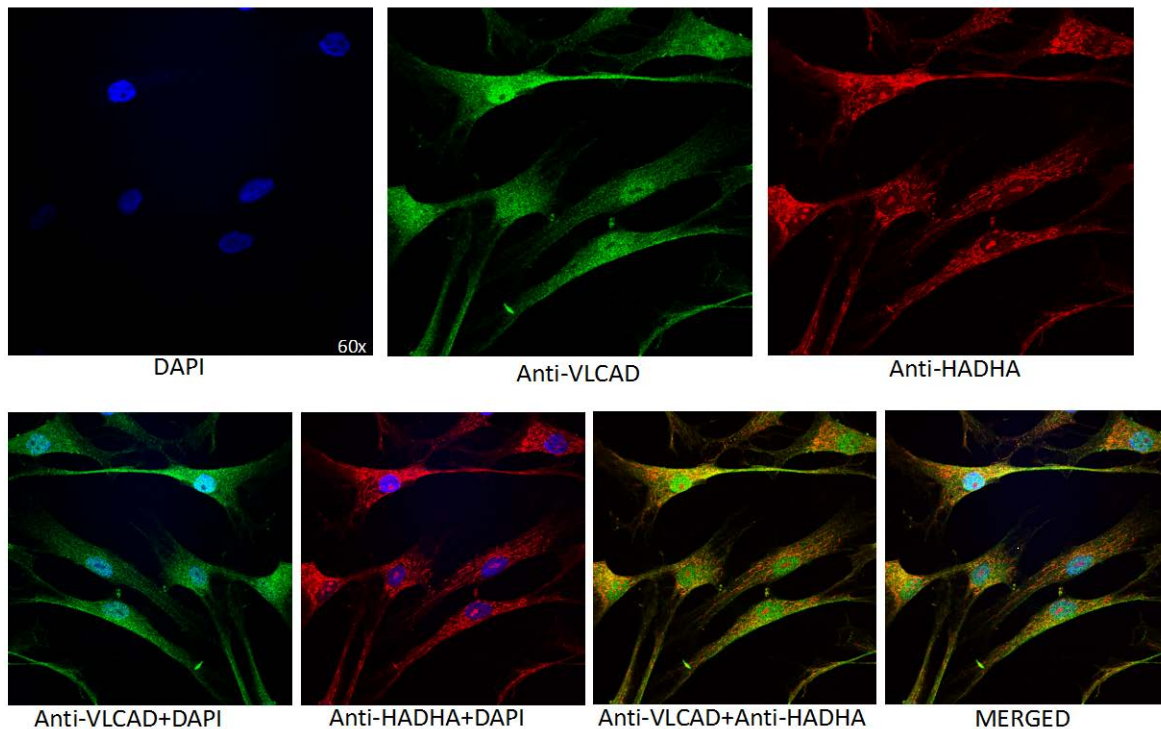
Figure 12. Typical confocal microscopy imaging of FAO enzymes.

Top row: DAPI, or nuclear stain, is shown in blue; staining with a VLCAD antibody is shown in green; and staining with an HADHA antibody is shown in red. Bottom row: merged combinations. Significant co-localization is shown in yellow. Co-localization can be implied at a resolution of ~200nm.

Figures 13 and 14 show results of STED imaging. The yellow merged signal indicates that HADHA (of TFP) and VLCAD are close enough to be physically interacting. Figure 15 shows a negative control using antibodies for TOM20 (an outer mitochondrial membrane

protein) and ATP5B (an inner mitochondrial membrane protein). As expected, these protein subunits show no co-localization at STED resolution.
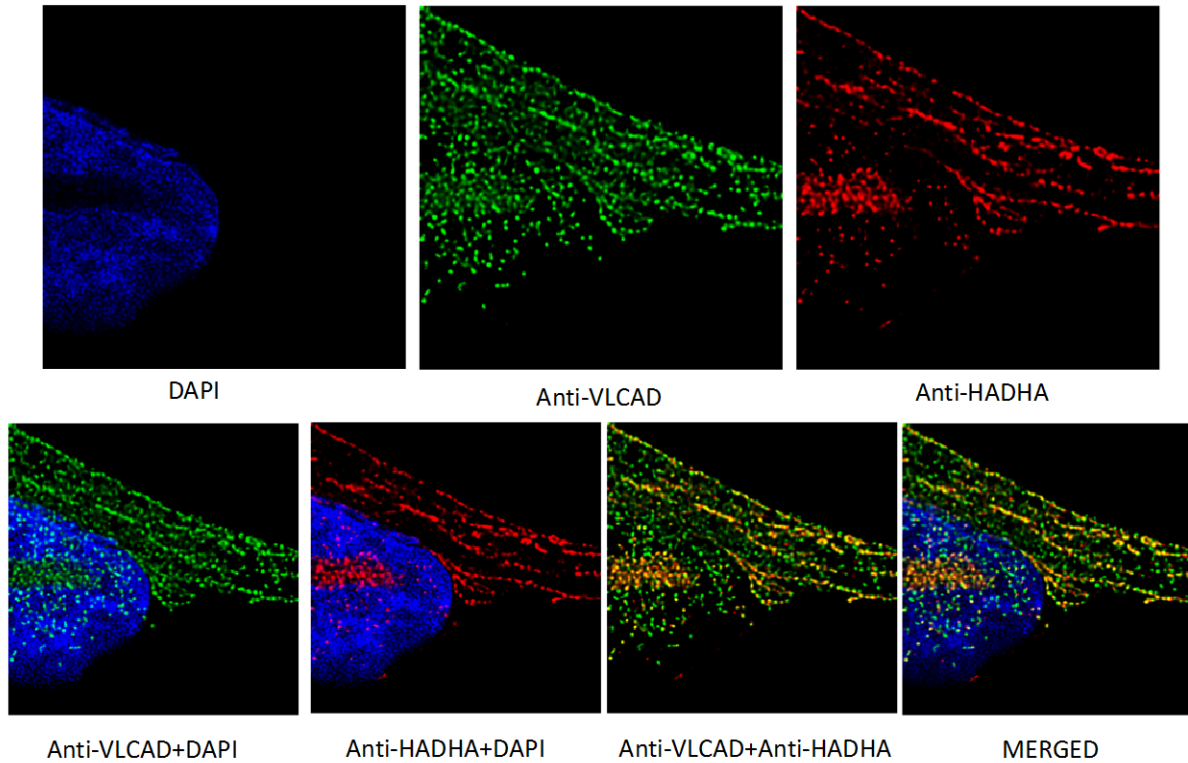
Figure 13. STED microscopy image example using FAO enzymes.

Top row: DAPI, or nuclear stain, is shown in blue; VLCAD is shown in green; and HADHA is shown in red. Bottom row: all merged combinations. Significant co-localization is shown in yellow. Co-localization can be implied at a resolution of <60nm.

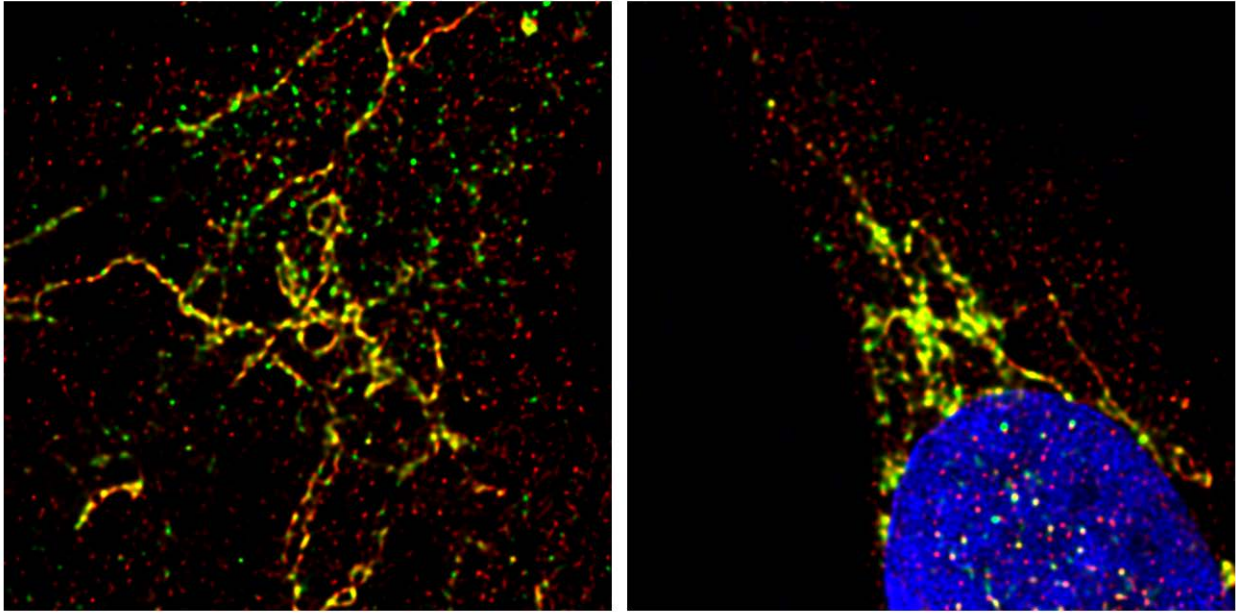**Figure 14. Merged images of FAO enzymes co-localizing using STED.**

Following the same color scheme as in Figures 12 and 13, a significant amount of yellow indicated significant co-localization between TFP and VLCAD at a resolution of <60 nm using STED.
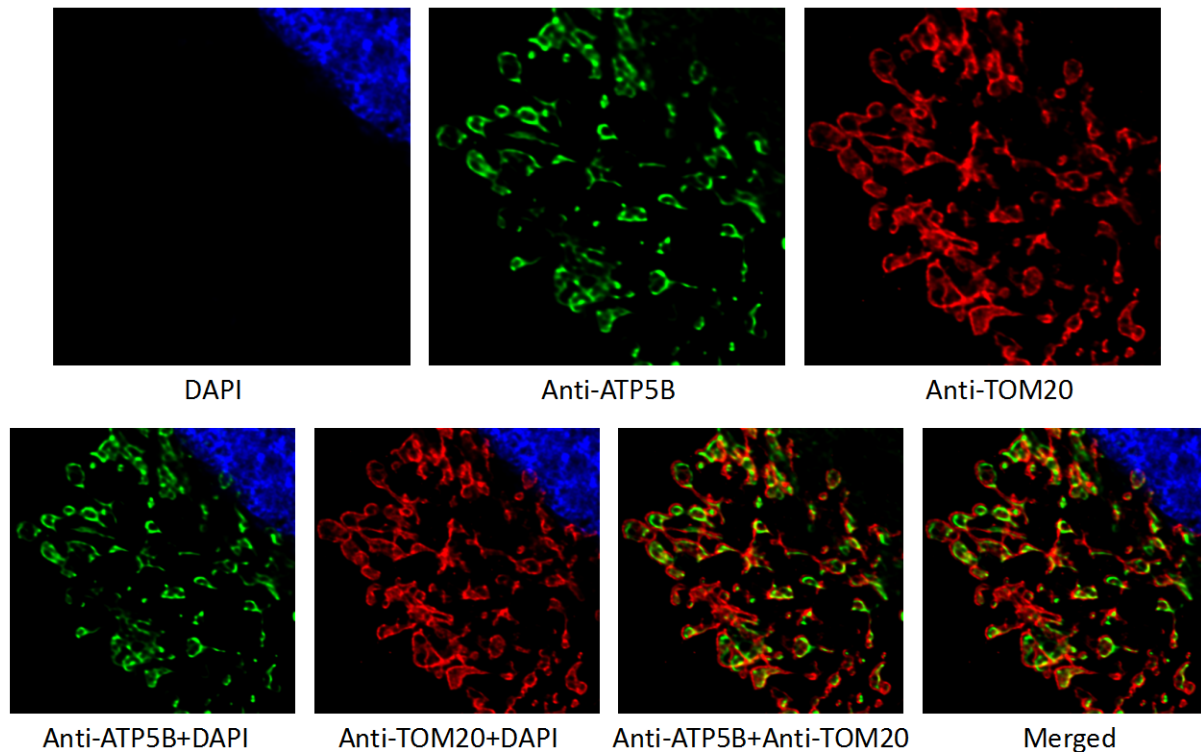
Figure 15. Negative control stain for STED imaging.

DAPI shown in blue; ATPB5 (inner mitochondrial membrane bound protein) shown in green; TOM20 (outer mitochondrial membrane bound protein) shown in red. Little to no yellow is seen in the final merged images.

Because fibroblast cells have a relatively sparse number of mitochondria, HEPG2 cells were instead used for STED imaging to assess BCAA protein interactions. Cells were seeded as a monolayer on a glass cover slide and imaged with a variety of antibodies to BCAA metabolic proteins. In all cases, as a control, the same protocol was carried out but without the primary antibody so that background fluorescence measurements could be taken. Note that not all commercially available antibodies were suitable for STED imaging. Therefore, all combinations of BCAA subunits could not be tested. Antibodies to IVD and MCCC2 (Figure 16) show co-localization of these proteins involved in consecutive steps in the LEU degradative pathway. Three-dimensional reconstruction videos of these images are available online. These results are

consistent with the findings obtained in Specific Aim 1a. Next, IVD and SBCAD antibodies were used for staining (Figure 17). This combination of antisera shows little to no co-localization, again consistent with earlier results. In the proteomic results above, IVD is present in high molecular weight bands; however, SBCAD does not co-migrate with IVD on a gel. Together, these results suggest that proteins of the LEU degradative pathway interact, but that they do not interact with those of the ILE pathway.
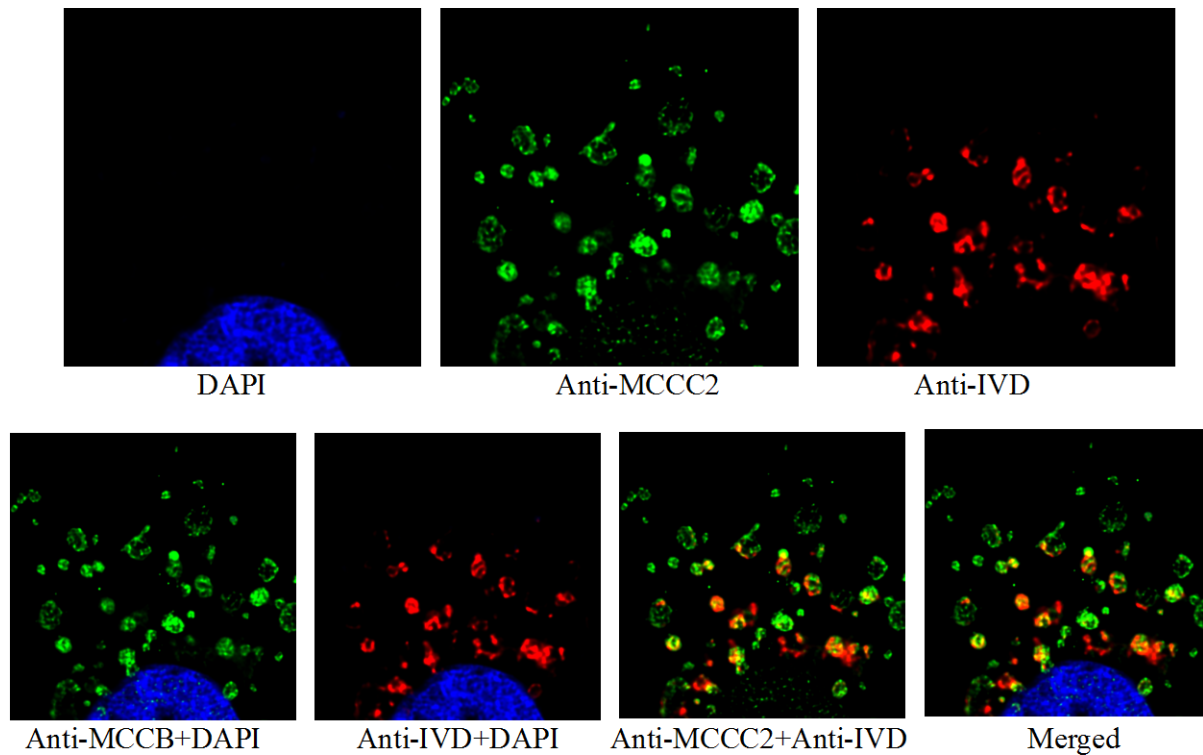
Figure 16. IVD and 3MCC show co-localization using STED.

DAPI is shown in blue; MCCC2 is shown in green; IVD is shown in red. Upon close examination of the bottom right merged images, one can see many instances of co-localization between the two enzymes of the LEU degradative pathway. The mitochondrial architecture is visible at a resolution of <60 nm.
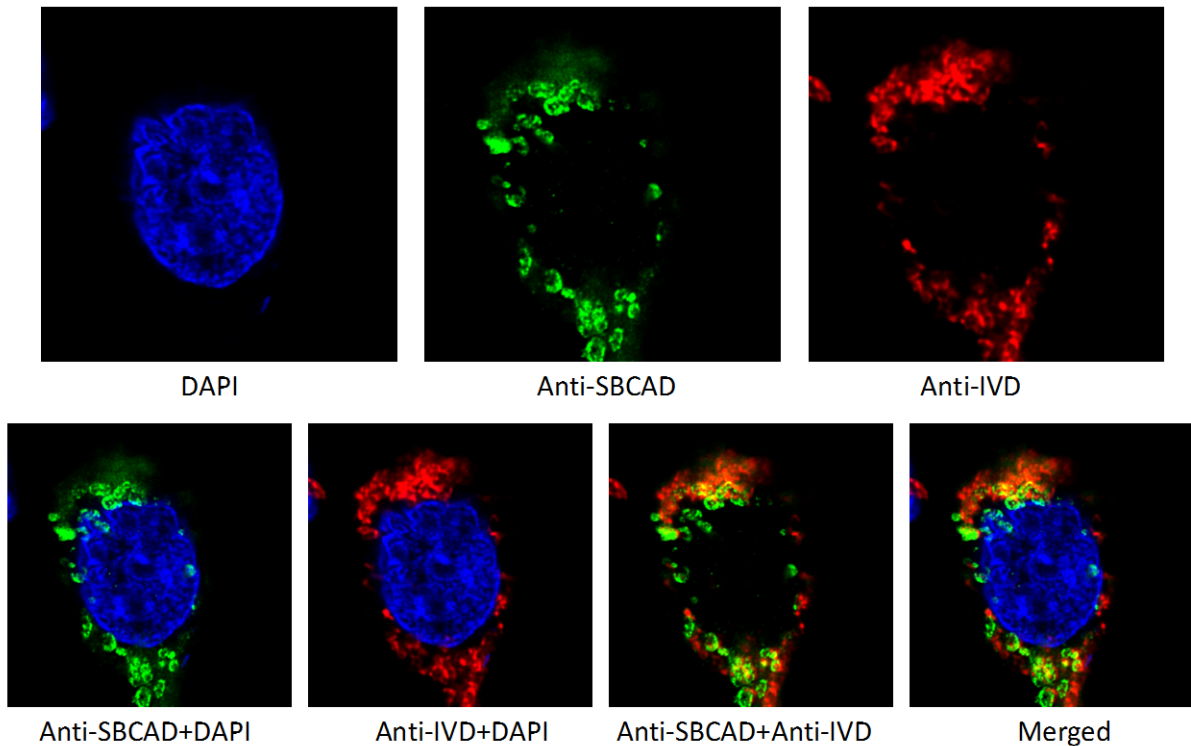
Figure 17. IVD and SBCAD do not show co-localization using STED imaging.

DAPI is shown in blue; is SBCAD shown in green; is IVD shown in red. Upon close inspection, little yellow is seen in the final merged images. A comparison of the individual images at the top reveals that these two ACADs are seen in different locations in the mitochondria. Resolution of <60 nm.

2.3   DISCUSSION

The cellular cross linking and western blot findings suggest that some of the BCAA enzymes interact to form a protein complex. Such a complex could promote metabolic channeling. Proteomics experiments with mass spectrometry supports the western results since multiple proteins involved with the BCAA metabolic pathways were identified in higher molecular bands after cross-linking. Figure 18 summarizes the proteins found in high molecular mass bands mapped onto the BCAA catabolic pathway. Here, the difference between the cross-linked and

control samples is clear, with many more BCAA metabolic proteins identified in cross linked samples. As noted briefly above, these findings alone do not differentiate between a common complex encompassing all BCAA pathways or individual complexes for each BCAA pathway. However, the STED results show that IVD and 3MCC interact with each other, while IVD and SBCAD do not, suggesting that the enzymes for the LEU and ILE pathways are in separate complexes.

Of note, in MS studies IVD is found as a lower molecular mass monomer without cross-linking, and in higher molecular mass complexes with cross-linking. However, SBCAD (noted as its gene name *ACADSB* in Figure 10 above) is not identified as participating in a larger complex. Additionally, IBD is not identified at all through MS analysis, a finding that requires additional study to understand.

One major question about the clinical significance of genetic disorders of the branched chain ACADs is not answered by these studies. IVA is the most severe of the three deficiencies, while SBCAD deficiency is asymptomatic and IBD deficiency is nearly so; however, the reason for this difference is unclear. One possibility is that isovaleryl-CoA and its alternative metabolites are more toxic than those of 2-methylbutyryl- and isobutyryl-CoA. In this case, metabolic channeling would have nothing to do with the phenotype of each disease. In contrast, it may be that enzymes that can alternatively metabolize substrates accumulating to blunt their toxicity. In this scenario, one would expect that these enzymes would need to be physically in proximity to the mutant's enzyme, otherwise, the concentration of the accumulating metabolite would not reach a high enough level to be used as an alternative substrate by another enzyme. My results show that IVD and SBCAD do not interact, thus potentially explaining the relatively severe symptoms seen in IVA. In addition, isovaleryl-CoA is not utilized by IBD and SBCAD.

In contrast, IBD and SBCAD utilize each other's substrates, and if they interact, then the local concentration of each blocked metabolite would become high enough to allow it to be utilized by the other enzyme. Additional STED experiments will be necessary to evaluate this possibility.
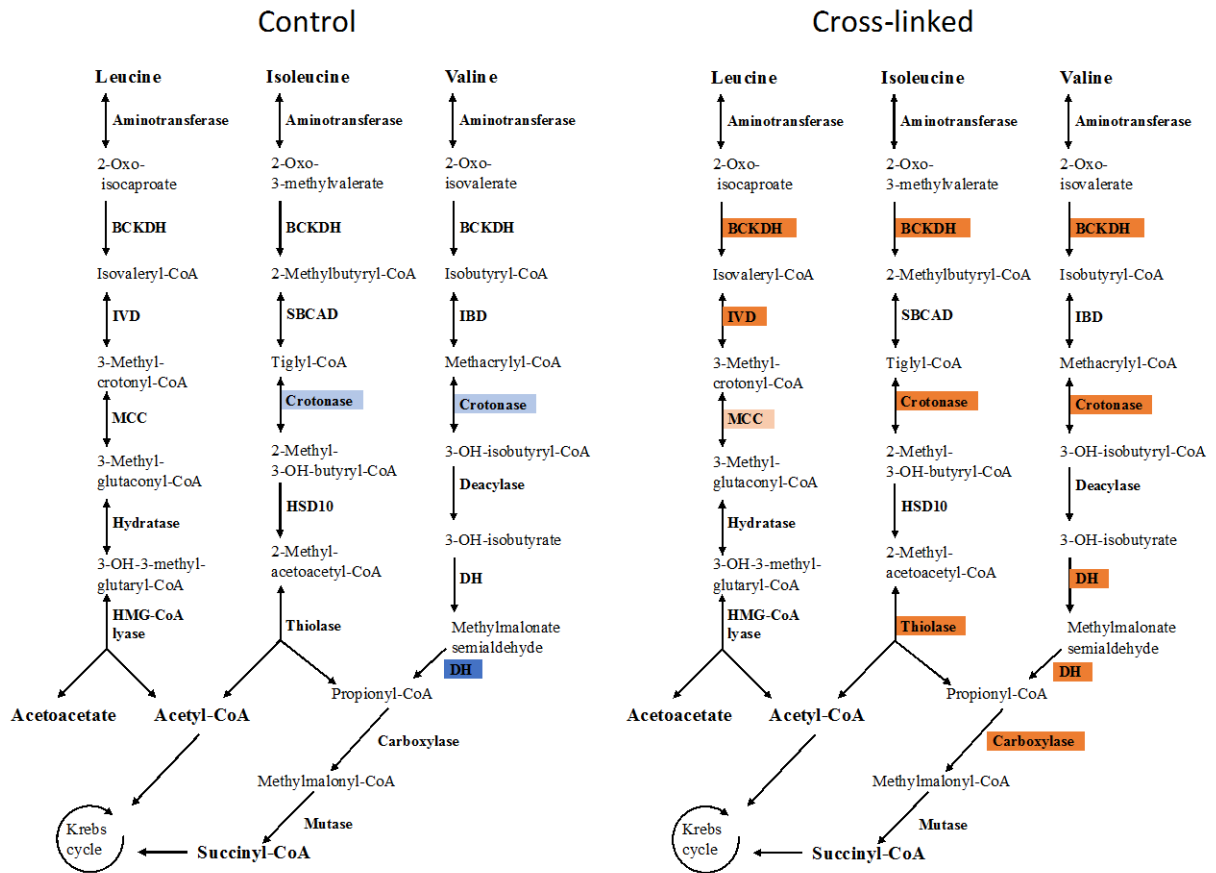
Figure 18. Mapped BCAA proteins based on proteomic and imaging results.

The presence of BCAA proteins as seen in my proteomic studies are mapped to the BCAA catabolic pathway. The left shows the lack of protein subunits observed at high molecular mass in control gel slices, while the right pathway maps the BCAA subunits observed in gel slices that have been exposed to chemical cross-linking. Filled boxes of blue or orange indicate the holoenzyme is present and the light shaded boxes indicate only a subunit of the holoenzyme was detected via MS.

Co-localization of IVD and 3MCC in a protein complex could have significant implications for therapy of both disorders. Molecules that stabilize such a macro molecular complex could improve residual activity of a mutant enzyme and increase flux through the pathway. Alternatively, developing methods to shunt the metabolites to another pathway with an overlap in substrate specificity would decrease accumulation of the abnormal metabolite and reduce its toxicity. Thus, additional experiments to explore the physical relationships of the BCAA pathway enzymes will be of interest.

3.0   A BCAA SUPER-COMPLEX AFFECTS METABOLIC FLUX

3.1   MATERIALS AND METHODS

Materials

Growth media   – 500 mL DMEM + 5% (25 mL) dialyzed FBS + 5 mL L-glutamine + 5 mL penicillin/streptomycin

Labeled media   – 100 mL growth media + 50% isotope enrichment:

LEU   – 10.9 mg $^{13}C6,^{15}N$ LEU + 10.5 mg ILE + 9.4 mg VAL; Cambridge Isotopes; Cat#CNLM-281-H-0.1

ILE   – 10.9 mg LEU + 10.5 mg $^{13}C6,^{15}N$ ILE + 9.4 mg VAL; Cambridge Isotopes; Cat#CNLM-561-H-0.1

VAL   – 10.9 mg LEU + 10.5 mg ILE + 9.4 mg $^{13}C6,^{15}N$ VAL; Cambridge Isotopes; Cat#CNLM-442-H-0.25

Heptanoate – 6 µL 5,6,7-$^{13}C3$ heptanoate; Aldrich; Cat#606499-0.10G

MET   – 7.7 mg $^{13}C5$ MET; Cambridge Isotopes; Cat#CLM-893-H-0.05

THR   – 9.5 mg $^{13}C4$ THR; Cambridge Isotopes; Cat#CLM-2261-0.1

GLN   – 7.65 mg $^{13}C5$ GLN (Cambridge Isotopes; Cat#CNLM-1275-H-0.1) in 100 mL RPMI media containing no L-glutamine (Corning; Cat#15-040-CV)

Extraction buffer   – 80 mL MeOH + 20 mL H_2O (HPLC grade)

Ammonium carbonate – 7.2 g ammonium carbonate + 1 L H_2O; pH to 7.5 with acetic acid

Time points   – 0, 10, 30, 60, and 180 min

Table 6. Characteristics of control and patient derived fibroblast cell lines tested.

	Identifier	Phenotype	Gene affected	Genetic mutation	Protein change	Passage range	Available patient characteristics
1	Fb554	Wild type	N/A			5-10	8 yrs old, male
2	Fb118	IVA	*IVD*	149G>C	21R>P	6-10	10 days old, consanguineous parents
3	Fb482	IBD deficiency	*ACAD8*	455T>C	152M>T	2-10	
4	Fb589	SBCAD deficiency	*ACADSB*	443C>T	148T>I	2-10	Female
5	Fb860	MSUD	Unknown			2-7	
6	Fb861	PPA	*PCCA*	Unknown		2-10	
7	Fb858	MMA	*MUT*	Unknown		12-15	

Stable isotope labeling

WT and organic aciduria patient derived fibroblast cell lines were obtained and grown in T175 culture flasks until 90% confluence. On day 1 of the protocol, cells were trypsinized, counted, and seeded at approximately 150,000 cells/well of three 6-well plates (Table 7). On day 2, complete DMEM media was removed and cells were fed with DMEM media containing 5% dialyzed FBS. On day 3, the labeling studies were performed. First, 1 hr prior to the first 180 min time point, the media in the T175 flask was refreshed with 5% dialyzed FBS DMEM. Before the first 180 min time point, 100 mL fresh media containing uniformly $^{13}C,^{15}N$-labeled amino acid and 500 mL fresh ammonium carbonate wash were made. Both solutions were placed in a 37 °C water bath to completely dissolve the substrates. The labeled media was vacuum filtered. Growth media was aspirated from wells for the first time point (180 min). The wells were washed with ~2 mL ammonium carbonate for <1 min and aspirated fully. 2.5 mL labeled media was added to cells for first time point and incubated in a 37 °C/5.0% CO_2 incubator. Wash and incubation for each time point was repeated at 60, 30, and 10 min time points. No label was added to the 0 min

time point. In between time points, cell counts in triplicate wells were measured with a Vi-Cell instrument. At the end of all time points, all wells were briefly washed with ammonium carbonate. Extraction buffer was added in a 1 µL/1,000 cell ratio and incubated on dry ice or -80 °C for 10 min. The extraction buffer was removed and saved in labeled Eppendorf tubes, with special attention to obtain as much extract as possible. Samples were centrifuged at 12,000 rpm for 10 min in 4 °C. Supernatant of samples were then transferred to a 96-well plate (Table 8). Finally, the wells were dried in a vacuum centrifuge (>1 hr). The plate was wrapped in Parafilm, clearly labeled with date, experiment, and name, and stored in -80 °C.

Table 7. 6-well plate layout for metabolic flux studies.

	1	2	3
A	Time point 180, Time point 30, Time point 0	Time point 180, Time point 30, Time point 0	Time point 180, Time point 30, Time point 0
B	Time point 60, Time point 10, Cells to count	Time point 60, Time point 10, Cells to count	Time point 60, Time point 10, Cells to count

Table 8. 96-well plate layout for MS analysis of cell extracts.

|	1	2	3	4	5	6	7	8	9	10	11	12
A	WT/LEU - Time point 0 min			WT/LEU – Time point 10 min			WT/LEU – Time point 30 min			WT/LEU – Time point 60 min		
B	WT/LEU – Time point 180 min											
C	WT/Experimental label – Time point 0 min			WT/Experimental label – Time point 10 min			WT/Experimental label – Time point 30 min			WT/Experimental label – Time point 60 min		
D	WT/Experimental label – Time point 180 min											
E	Experimental condition 1 – Time point 0 min			Experimental condition 1 – Time point 10 min			Experimental condition 1 – Time point 30 min			Experimental condition 1 – Time point 60 min		
F	Experimental condition 1 – Time point 180 min											
G	Experimental condition 2 – Time point 0 min			Experimental condition 2 – Time point 10 min			Experimental condition 2 – Time point 30 min			Experimental condition 2 – Time point 60 min		
H	Experimental condition 2 – Time point 180 min											

Result analysis

96-well plates were analyzed via orbitrap mass spectrometer. The protocol was carried out in collaboration with Agios Pharmaceuticals and has been described in literature previously[55].

3.2   SPEIFIC AIM 2: RESULTS

3.2.1   An IVD deficient cell line produces acetylcarnitine from LEU

Specific Aim 2 was to characterize metabolic channeling through the BCAA pathways. Here, I focused on flux through the branched chain amino acid pathways in fibroblast cell lines derived from controls and patients with genetic disorders in the pathway (Table 8). These experiments were performed in collaboration with scientists at Agios Pharmaceuticals. First, wild type or mutant cells were grown in media supplemented with $^{13}C,^{15}N$ isotopes of LEU, ILE, or VAL for 0, 10, 30, 60, and 180 min. The reactions then were quenched and washed with ammonium carbonate, and cellular lysates were extracted at -80 ^{o}C with 80/20 MeOH/H_2O. As a control, cells were grown with $^{13}C,^{15}N$ labeled LEU for every experimental run. All samples were lyophilized then sent to Agios for metabolite analysis by tandem mass spectrometry. Figure 19 shows results from wild type and IVA cell lines grown in labeled LEU. As expected, isovalerylcarnitine accumulated in the IVD deficient but not wild type cells. In contrast, the IVD deficient cells show a small accumulation of acetylcarnitine, the end product of LEU catabolism, compared to wild type cells. Since the IVD deficient cell line had a null 149 G>C mutation[56] shown to have no immune-detectable IVD protein, production of any end-product is unexpected. This result indicates alternative metabolism of the labeled isovaleryl-CoA from LEU, a potential sign of low level metabolic cross-correction by one of the other BCAA catabolic pathways.
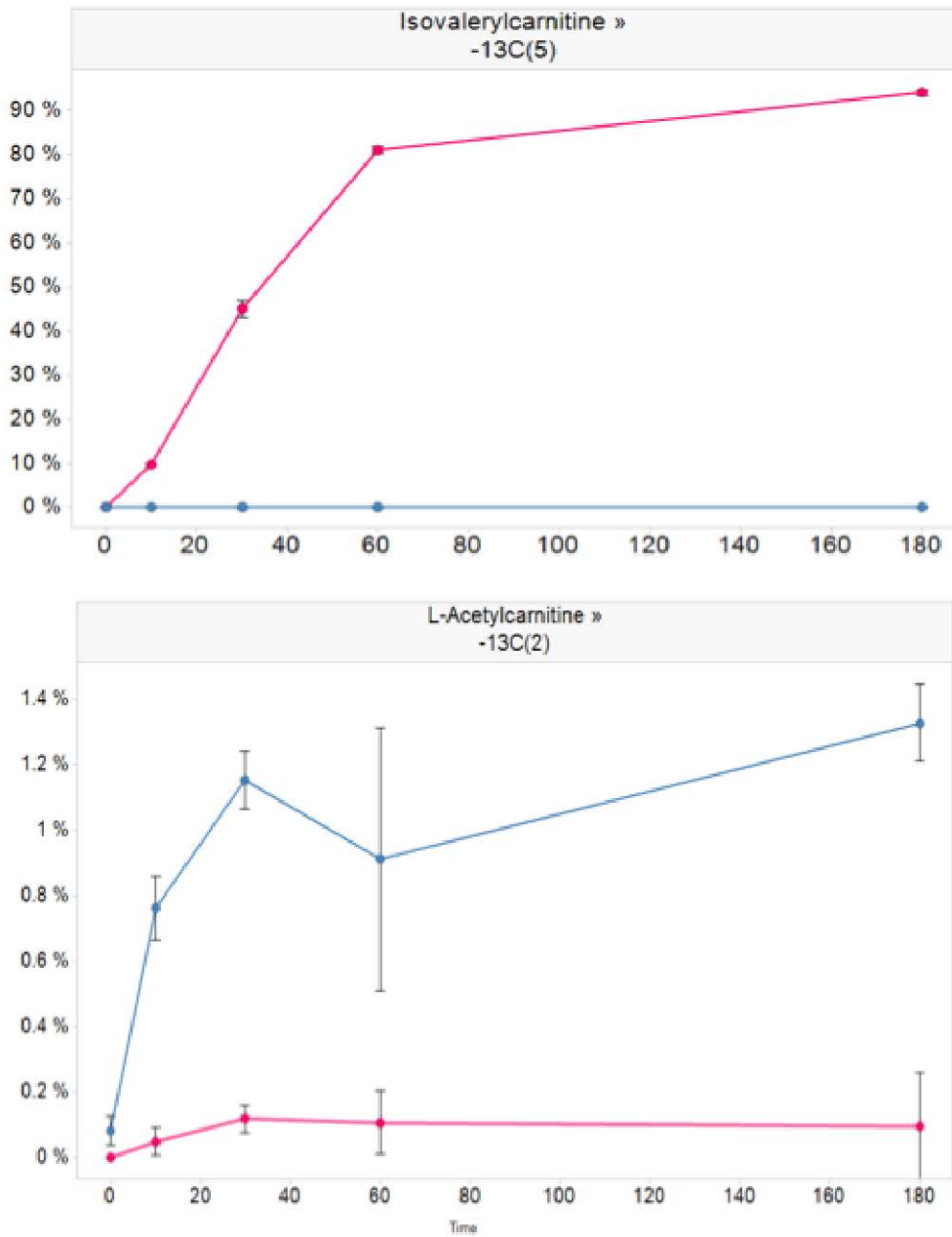
**Figure 19. IVD cells fed labeled LEU show labeled end-product.**

The red line represents the WT cell line and the blue line represents the IVA patient derived cell line. The vertical axes measure the corrected percentage of the acetylcarnitine pool derived from the label. As described in the text, any amount of acetylcarnitine accumulation in the IVD cell is of significance due to its null mutation.

3.2.2   SBCAD and IBD deficient cell lines generate propionylcarnitine from ILE and VAL

To examine metabolic flux through the ILE and VAL pathways, IBD and SBCAD deficient cell lines were grown in stable isotope labeled VAL and ILE, respectively, as in the previous section (Figure 20). The IBD cell line contained a mutation at 455T>C and the SBCAD cell line contained a mutation at 443C>T. The mutations in both patient cell lines caused complete deficiency in the enzyme[57,58]. When SBCAD deficient cells were grown in labeled ILE, ~15% of the total propionylcarnitine pool was derived from the labeled ILE (Figure 20A). In all experiments performed, labeled substrate was added to 50% enrichment. For example, standard DMEM media contains 0.8 mM of LEU, so to test BCAA metabolics and increase flux, 0.8 mM $^{13}C,^{15}N$-labeled LEU was added to the media. Thus, the effecive percentage of labeled end product seen in Figures 20 and 21 can be doubled due to the 50% enrichment of the label. When IBD cell lines were grown in labled VAL, 2% of the cellular propionylcarnitine was derived from the labeled VAL (Figure 20B). Again, this number can effectively be doubled to represent the amounts of VAL derived propionylcarnitine. When a WT cell line was grown in the presence of labeled ILE, >20% of the propionylcarnitine pool was labeled (Figure 21), incidating that a large proportion of the cellular propionate pool derives from ILE.
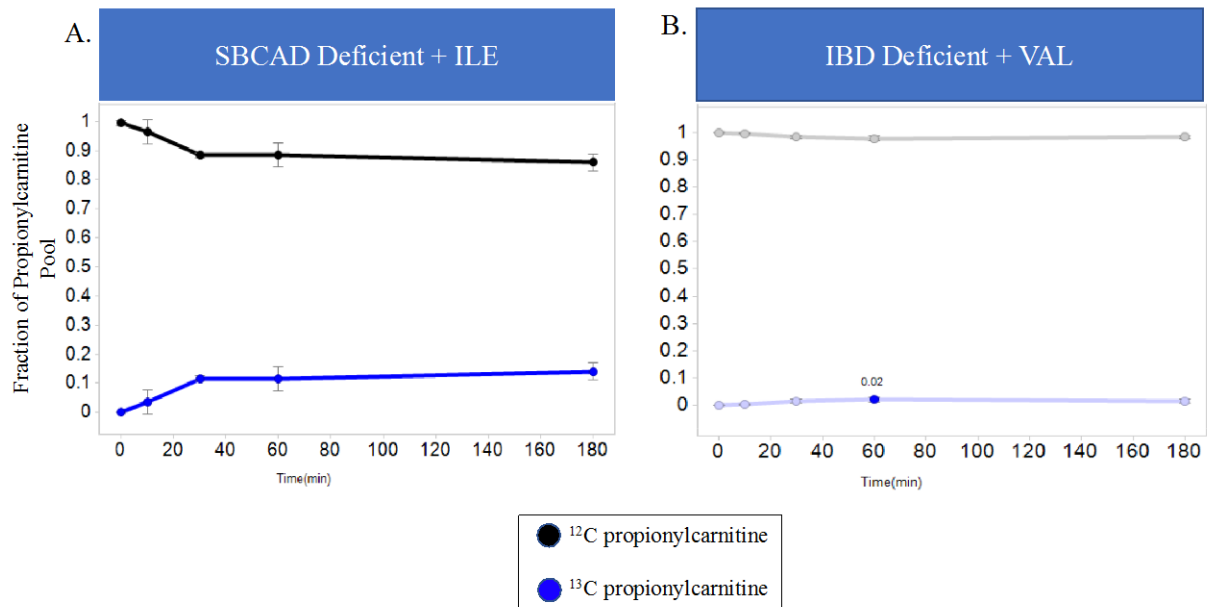
Figure 20. SBCAD cells fed labeled ILE and IBD cells fed labeled VAL produces labeled propionylcarnitine.

The black and gray lines represent the amount of ^{12}C propionylcarnitine in the cullular extract, and the blue lines respresent the ^{13}C propionylcarnitine in the extract derived from the added label. As noted in the text, ILE appears to be a larger propiogenic metabolite of the BCAAs than VAL.
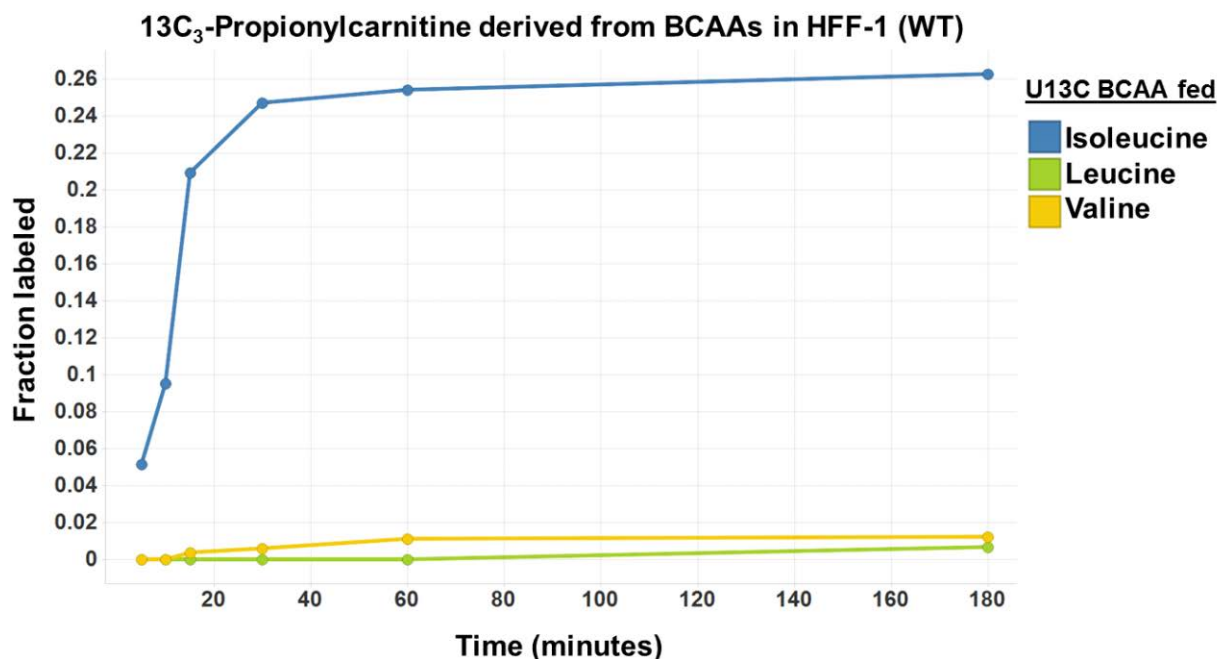
Figure 21. BCAA contributors to labeled propionylcarnitine.

Individual contributors of propionylcarnitine. Labeled BCAAs were added to HFF-1 cells and fraction of propionylcarnitine pool derived from the labeled was analyzed. ILE is a higher contributor to propionylcarnitine than VAL.

3.2.3 Propiogenic metabolites contribute differently to the propionyl-CoA pool

These results suggest that each of the popiogenic amino acids contribute differentially to the intracellular propionate pool, an issue of importance when considering dietary management of patients with propionic and methylmalonic acidemias. To further examine this issue, wild type cells were separately cultured in media supplemented with universally labeled VAL, MET, ILE, or THR, and accumulation of propionylcarnitine was measured. The cells were also grown in the presence of labeled $^{13}C3$-5,6,7-heptanoic acid, another propiogenic compound. Figure 22 shows the accumulation of propionylcarnitine obtained with each labled substrate. Labeled VAL, MET, and THR produce little to no measurable propionylcarnitine. The major contributors to the

propionate pool were ILE and the C7 fatty acid, a result that could impact the treatment of patients with propionic and methylmalonic acidemias. Note that the 0 min time points for VAL and THR showed a non-zero accumulation of labeled propionyl-carnitine accumulation, which is imposible as no label was added to the cells for this time point. The amount of label generated in the 0 min time point was then subtracted from the remaining time points, hence a negative accumulation of labeled proionylcarnitine.
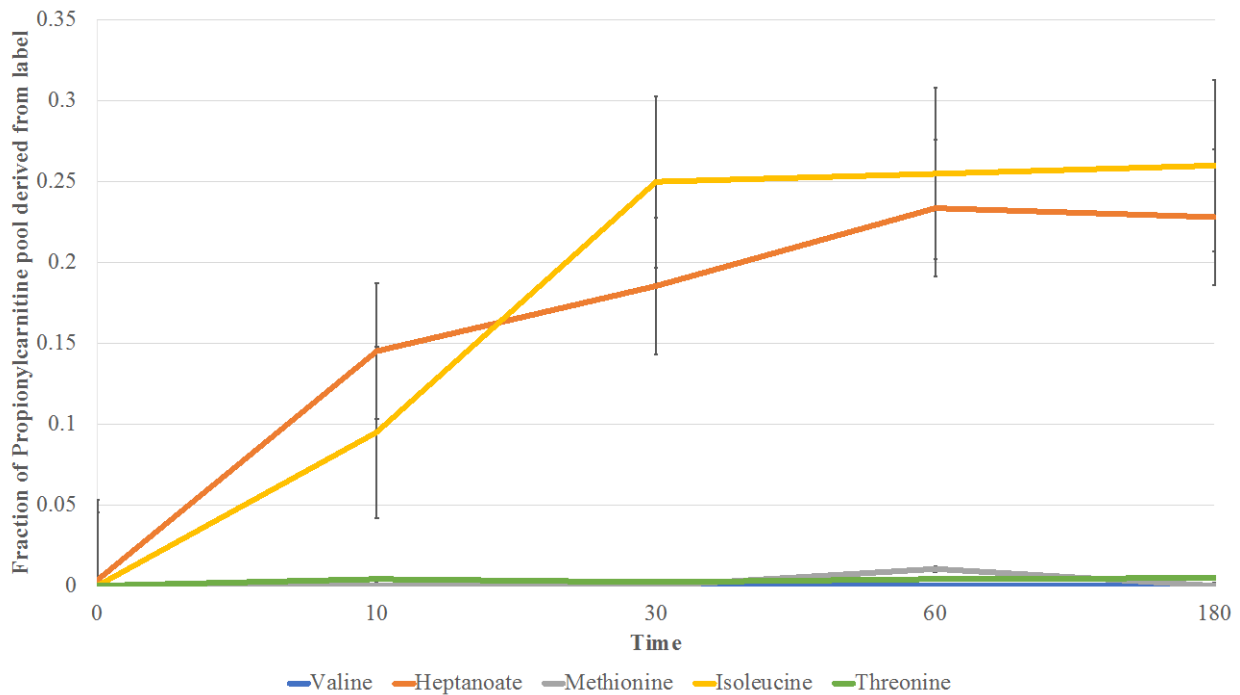
Figure 22. Differential contributions from propiogenic substrates to the propionylcarnitine pool.

Vertical axis represents the percent of total propionylcarnitine in WT cells that is derived from the labeled substrate. As seen above in Figure 21, ILE contributes the most to propionylcarnitine. Heptanoic acid also plays a role in the generation of propionylcarnitine, but the remaining substrates exhibit zero accumulation of the propionylcarnitine.

3.3   DISCUSSION

Specific aim 2 took a different approach to identify interaction of BCAA enzymes: looking for evidence of functional cross talk across metabolic pathways. These experiments took advantage of the availability of cell lines with deficiencies in IVD, SBCAD, and IBD. In these cells, production of the *bona fide* end product of catabolism, when metabolism of the precursor amino acid pathway is blocked, suggests shunting to another pathway. Thus, the production of labeled end products seen in these experiments is significant, suggesting that the alternative enzymes are physically close enough to allow reaction with the other promiscuous ACADs. For example, since 15% of the propionylcarnitine in SBCAD cell lines incubated with labeled ILE is labeled, it seems likely that the labeled, blocked 2-methylbutyryl-CoA is being acted upon by IVD or, more likely based on substrate specificity, IBD. Direct channeling of substrates is much more energetically favorable than catching and releasing substrates, especially sub-optimal ones; and, therefore, lends credence to the hypothesis of a BCAA protein complex encompassing at least the ILE and VAL pathways. As a much lower amount of label from LEU finds its way to acetylcarnitine, the IVD metabolon may be distinct form the ILE/VAL one, consistent with findings from Specific Aim 1. As described in the previous section, STED imaging would help to confirm this conclusion.

Of note, the flux experiments demonstrating that ILE and C7 dominate the contribution to the propionate pool have immediate potential clinical relevance. Patients with propionic and methylmalonic acidemias are treated with harsh dietary restrictions of VAL, MET, ILE, and THR as a means to reduce propionyl-CoA production. Since ILE contributes to the propionyl-CoA pool by ~10 fold over VAL, THR, and MET, patients likely need only to be restricted of ILE, simplifying their dietary management. One unanswered question remains the fate of

propionyl-CoA generated from VAL, MET, and THR. This question is explored in Future Directions below.

4.0   A NOVEL TREATMENT FOR PROPIONIC ACIDEMIA

4.1   INTRODUCTION

The focus of this chapter shifts from the BCAA ACADs discussed previously to PPA/MMA. As noted above, PPA and MMA affect approximately 1:100,000 patients each in the US. This number is increased in Chinese populations, and a visiting scholar, colleague, and collaborator, Dr. Bingjuan Han has focused her prior clinical work on the treatment of propionic and methylmolonic acidemia patients in China. Together with Dr. Han, the experiments performed in this section explored options for more effectively treating PPA. Current treatments rely largely on dietary restriction and liver transplantation with varying results. Given the loss of propionyl-CoA into the TCA cycle in this disorder, along with evidence of mitochondrial energy dysfunction, anaplerotic therapies, a supplantation of the TCA cycle, is a logical therapy. As seen in Figure 5, a block in PCC or MUT results in a loss of succinyl-CoA and subsequently succinate in the TCA cycle, reducing substrates for energy production, and increasing cellular stress.

Experiments in this section explore treatment of propionic acidemia fibroblasts with succinate as an anaplerotic agent and a cardiolipin binding peptide (CLBP) to act as a stabilization agenet of the inner mitochondrial membrane. CLPB is a proprietary molecule modeled on elamipretide currently used in clinical trials for treatment of respiratory chain defects and Barth syndrome[59]. This compound targets the mitochondria and stabilizes the repiratory

chain super-complex by interacting with the cardiolipin critical for inner mitochondrial membrane structure. The peptide has also been shown to act as an antioxidant and reduce ROS species in the mitochondria[60]. The CLBP could provide benefit to patients with PPA and MMA as both disorders have been proposed to induce mitiochondrial dysfunction.

4.2   MATERIALS AND METHODS

Materials

Protease inhibitor   – Life Tech; Cat#11836153001; 1 tablet/1 mL H_2O to obtain 10X

RIPA buffer   – Thermo Fisher; Cat#89901; 1 mL RIPA buffer + 100 µL 10X protease inhibitor

MitoSox   – 1 vial (50 µg) + 13.6 µL anhydrous DMSO = 5 M master solution; experimental concentration = 5 µM

MitoTracker   – 1 vial (40 µg) + 74.4 µL anhydrous DMSO = 1 mM master solution; experimental concentration = 0.15 µM

Sodium succinate   – Sigma Aldrich; Cat#S2378

Cardiolipin binding peptide – proprietary molecule based on elamipretide

Glucose-free media   – 50 mL FBS + 5 mL L-glutamine + 5 mL penicillin/streptomycin; life Technologies; Cat#11966-025

Whole cell lysate

WT, PPA, and MMA cell lines were grown in culture. PPA and MMA[61] cell lines were obtained from patients with a molecularly confirmed diagnosis. The cell culture protocol for detaching an adherent monolayer of cells was followed and a pellet was made from the detached cell suspension. The pellet can be stored at -80 ℃. Pellet was re-suspended with 150 µL of cold

RIPA buffer (including protease inhibitor – see above). The samples stood on ice for 30 min, vortexing every 10 min. The resulting mixture was centrifuged at 14,000 xg for 15 min at 4 $^{\circ}$C. Supernatant (lysate) was transferred to new vial for analysis on western blots. Traditionally, the Vockley lab uses < 20 µg of protein per lane for western blot visualization. Lysate can be stored in -80 $^{\circ}$C for long-term.

MitoSox/MitoTracker

From a 90% confluent T25 flask of fibroblasts, cell pellet was harvested for analysis by trypsinizing as described above, and cells/trypsin were suspended in 5 mL media. Samples were centrifuged at 500 xg for 6 min. The supernatants were removed, and the pellet was re-suspended in 850 µL complete DMEM media. Using a 1:10 dilution, cells were counted while preparing MitoSox and MitoTracker as listed above in "Materials." 45,000 viable cells were taken and suspended in media to make 200 µL of cell sample. 100 µL of MitoSox/MitoTracker master mix was pipetted to samples and incubated at 37 $^{\circ}$C for 20 min in 4 replicates. After incubation, cells were analyzed with via flow cytometry.

4.3   SPECIFIC AIM 3: RESULTS

4.3.1   Cardiolipin binding peptide decreases ROS production and mitochondrial mass in fibroblast PPA cells

Wild type, MMA, and PPA cells were grown in culture without glucose to increase reliance on oxidative phosphorylation for energy, supplemented to 4 mM succinate for 24 hrs, and cells were

harvested and assessed for reactive oxygen species and mitochondrial mass as a mesaure of cellular stress. Cells were counted, and incubated with MitoSox Red to measure reactive oxygen species and MitoTracker Green to measure mitochondrial mass in four replicates. Cells from a patient with PPA but not MMA showed an increase in ROS (Figure 23). Cells treated with succinate showed no statistically significant change in ROS production or mitochondrial mass (Figure 24). The PPA cells upon treatment with succinate for 24 hrs do show a statistically significant increase in ROS, suggesting persistant damage to the electron transfer chain.

Wild type, MMA, and PPA cells were grown again in culture without glucose, incubated with 100 nM cardiolipin binding peptide dissolved in DMEM media for 24 hrs, and cells were harvested and assessed for measurement of reactive oxygen species and mitochondrial mass. Incubation of cells with 100 nM CLBP reduced the levels of ROS in the PPA cell line, but not the MMA cell line (Figure 25). Similarly, CLBP treatment reduced the mitochondrial mass in PPA cells (Figure 26). Mitochondrial mass was near normal in MMA cells and did not change upon treatment with CLBP.
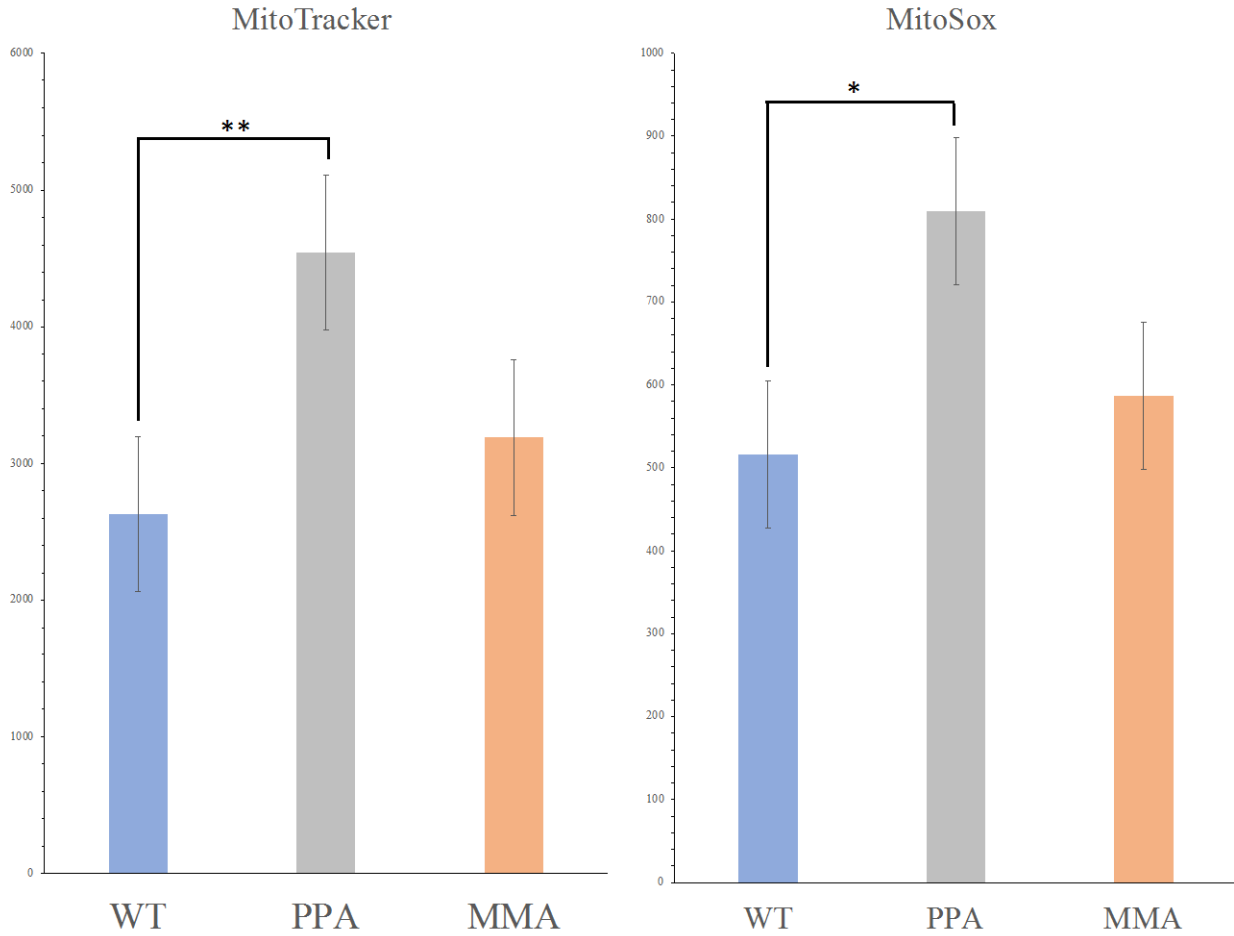
Figure 23. PPA experiences elevated ROS and mitochondrial mass as a marker for cellular stress.

MMA cell lines exhibited slightly elevated mitochondrial mass and ROS production, but not to significant levels. Colored bars represent means of four technical replicates for each cell line. Error bars represent standard error. Statistical significance determined by two-tailed t-test on all four sample replicates where $p < 0.05$ is considered significant as indicated by *s.
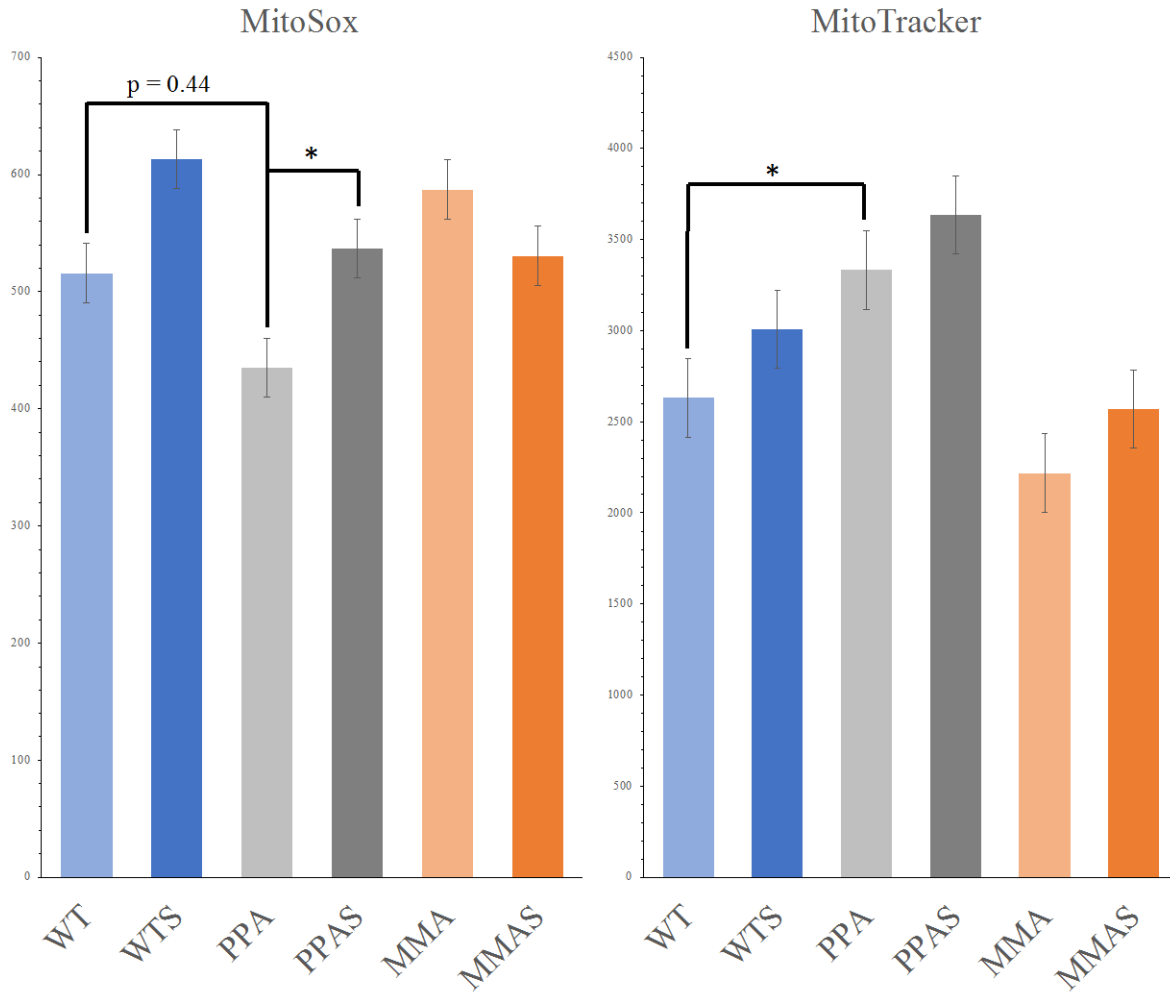
Figure 24. Succinate does not effectively decrease markers of cellular stress.

The dark shaded bars labeled with "S" in this graph represent the cell lines being treated with 4 mM of succinate for 24 hrs. MitoSox measures ROS, and MitoTracker measures mitochondrial mass. None of the changes between non-treated and treated cells seen were statistically, significantly decreased. Colored bars represent means of four technical replicates for each cell line. Error bars represent standard error. Statistical significance determined by two-tailed t-test on all four sample replicates where $p < 0.05$ is considered significant as indicated by *s.
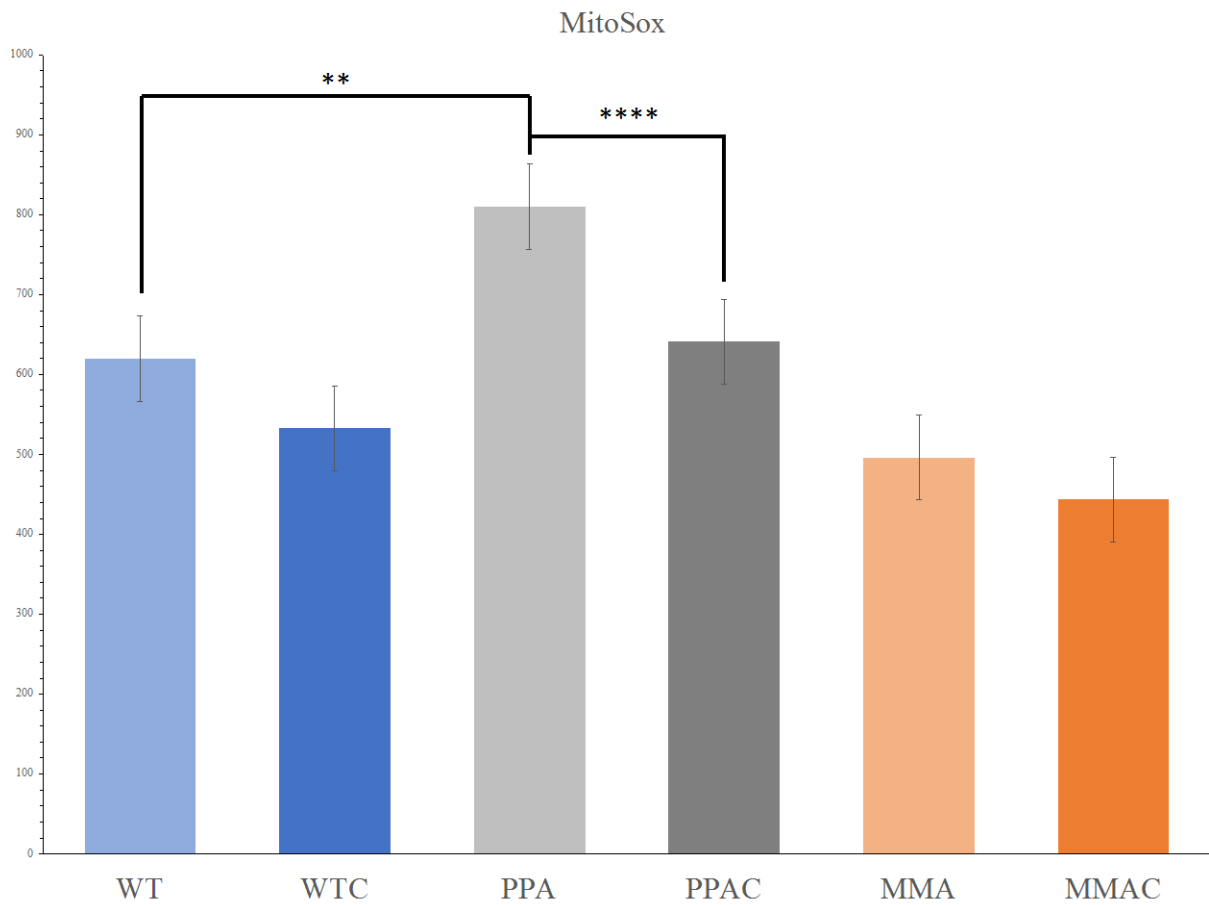
Figure 25. ROS production by cardiolipin binding peptide in PPA cells.

Again, dark bars labeled with "C" represent treatment of the cells for 24 hrs with the cardiolipin binding peptide. ROS production was elevated in PPA which was reduced to near normal when treated with CLBP. MMA ROS was not elevated. Colored bars represent means of three technical replicates for each cell line. Error bars represent standard error. Statistical significance determined by two-tailed t-test on all three sample replicates where $p < 0.05$ is considered significant as indicated by *s.
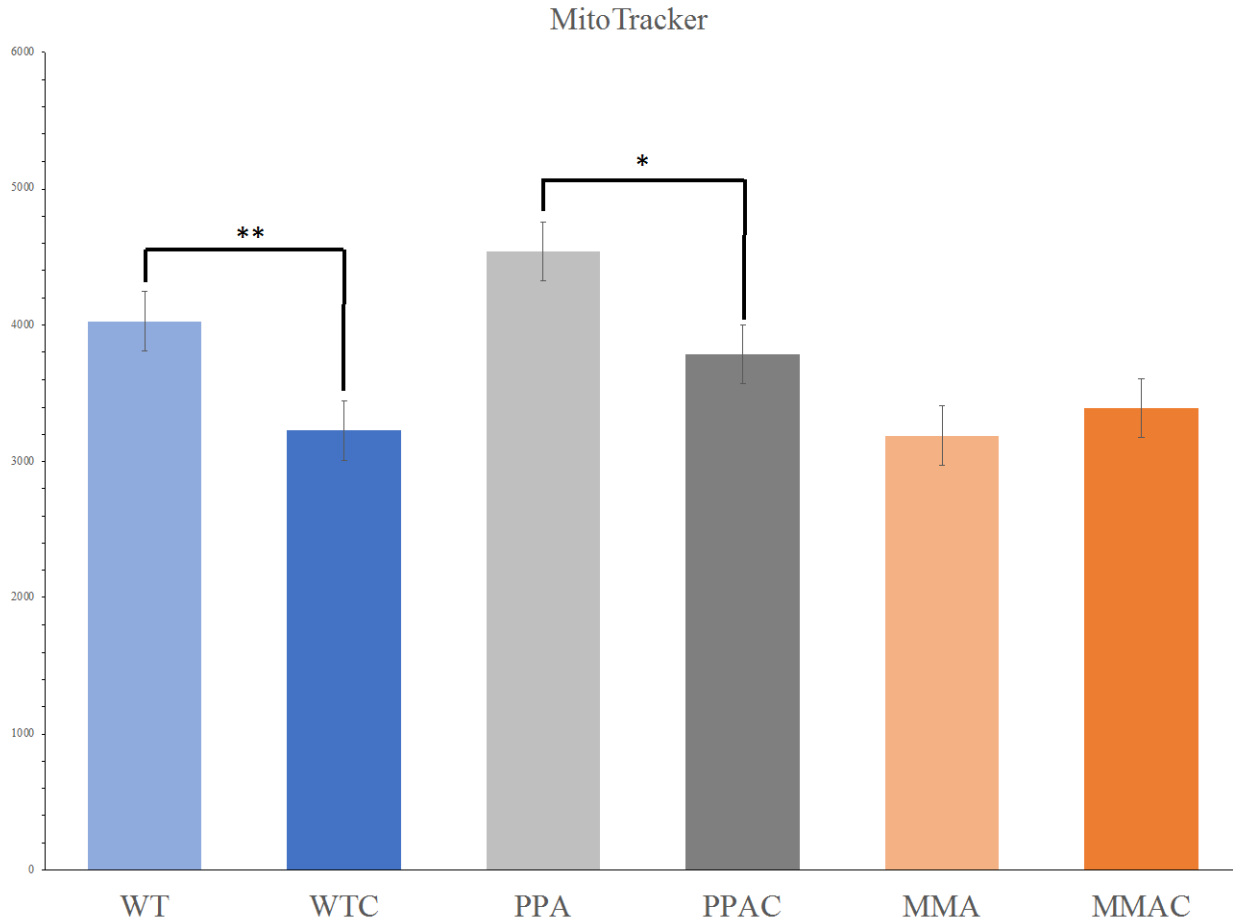
Figure 26. Mitochondrial mass reduced by cardiolipin binding peptide in WT and PPA cells.

Following the same pattern as seen in the previous two figures, note the statistically significant reduction in mitochondrial mass in both WT and PPA cell lines under the treatment of CLBP. Colored bars represent means of four technical replicates for each cell line. Error bars represent standard error. Statistical significance determined by two-tailed t-test on all four sample replicates where $p < 0.05$ is considered significant as indicated by *s.

4.3.2   Cardiolipin binding peptide increases PCC amount in PA fibroblasts

Wild type, PPA and MMA cells were grown in glucose free media to stress the cells and increase use of alternative energy sources such as BCAAs. Succinate or the cardiolipin binding peptide (CLBP) was then added directly to the cellular growth media and cells were grown for 24 hours. Cells were harvested, lysates were electrophoresed on SDS-PAG gels, and the gels were

transferred to PVDF membranes. PCCA and MUT proteins were visulized with streptavidin and a MUT specific atibody. (Note that streptavidin was used to visualize PCCA based on its strong avidity to biotin, a cofactor of PCCA. The streptavidin used in this experiment was directly conjugated to a fluorophore for western blotting.) Figure 27 shows that PCCA is decresed in the PPA cells compared to wild type, and that MUT is completely absent in the MMA cells. Succinate alone did not increase the level of PCCA or MUT. In contrast, cells incubated with CLBP showed increased PCCA, while MUT was unaffected.
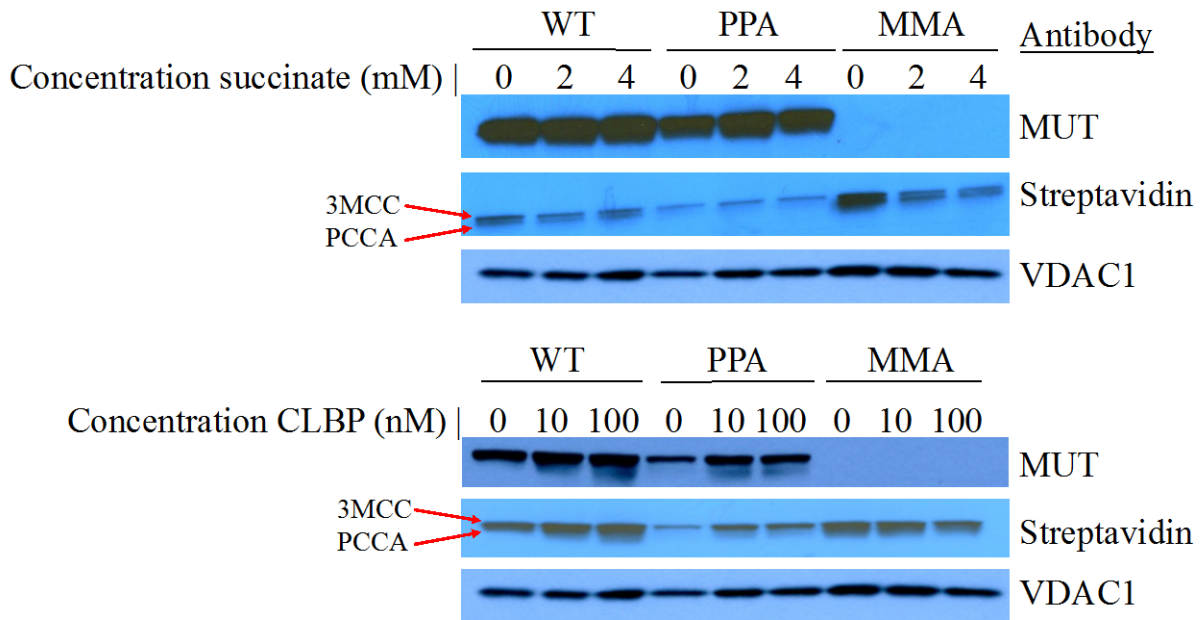
Figure 27. Western blot of succinate and cardiolipin binding peptide treatments.

Note that the streptavidin blot shows two bands in close proximity. The top band is that of MCCC1 of the LEU pathway which also utilizes biotin. The bottom band is of more interest in this context as it represents the PCCA subunit that is deficient in PPA patients and in this patient-derived cell line.

4.4   DISCUSSION

Elamipretide, an analogue of the CLBP used in these experiments, has been shown to interact with the inner mitochondrial membrane and stabilize mitochondrial respiratory chain supercomplexes. Stabilization of PCC in the PPA cells by the CLBP suggests that the PCC may also be part of a BCAA protein complex interacting with the mitochondrial membrane, consistent with findings in the previous two aims. These results, taken with those found in section 3, highlight a possible novel approach to PPA theraputics. Treatment with with fewer dietary amino acid restrictions (only ILE), along with addition of the CLBP to reduce the induction of secondary ROS, could provide better therapy to these patients. More studies will need to be performed to validate this novel treatment including measurement of cellular oxygen consumption rates, and animal model testing such as a labeled metabolic flux study.

5.0   OVERALL CONCLUSIONS AND FUTURE DIRECTIONS

The main conclusion of this thesis, is that branched chain amino acid metabolism likely occurs in one or more multi-protein complex(es) that promotes metabolic channeling. It would appear that mitochondria have developed multiple protein complexes that enhance metabolic channeling. This phenomenon is seen in the electron transport chain (ETC) which is organized into a super-complex for energy production. My results support the hypothesis that BCAA catabolism enzymes likely form two substrate-channeling, energetically-favorable protein complexes in the mitochondria, one for LEU catabolism and one for ILE and VAL. This finding may help explain the disparate symptoms seen in IVA vs isobutyryl and 2-methylbutyryl academia. In the case of IVA, the lack of another closely associated metabolon allows the isovaleryl-CoA accumulating behind the metabolic block to escape into the mitochondrial matrix and cause damage via interaction with other metabolic enzymes. In contrast, the metabolic consequences of SBCAD and IBD deficiencies, by virtue of close proximity to each other, could be abrogated by utilization of the alternate ACAD and return of the product to the appropriate pathway beyond the metabolic block. The known substrate promiscuity of SBCAD and IBD, and their utilization of each other's substrate relatively efficiently are consistent with this possibility. Interestingly, a recent study[62] reports that IVD shows a relatively high affinity for 2-methylbutylryl-CoA (K_m = 1.9 μM). This finding lends credit to my hypothesis that a build-up of 2-methylbutyryl-CoA causes insignificant metabolic changes due to substrate sharing by BCAA ACADs. In this case, a

block in catabolism of 2-methylbutyryl-CoA could be abrogated by IBD accepting the nearby metabolite in a larger shared ILE/VAL super-complex or by IVD accepting a released metabolite in its own LEU protein complex. Secondary disruption of the LEU catabolic complex by primary mutations in one protein of the complex may also play a role in the pathogenicity of IVA. Here, mutations that might leave some residual activity in the IVD protein could still lead to disruption of its interaction with other complex member proteins and ultimately lead to a more severe phenotype than predicted by the effect of the mutation on IVD activity alone. To test this hypothesis, one could use patient derived cell lines of varying genotypes and repeat the experiments presented in this dissertation. If the hypothesis of a LEU pathway metabolon is true, one would expect the more severe mutations in *IVD* based on patient reports to have significantly less co-localization with other BCAA enzymes than a WT counter-part. A less-severe, or asymptomatic patient-derived IVA cell line identified through newborn screening may show a similar amount of co-localization of IVD with proteins like 3MCC or the BCKDH complex as compared to controls. Alternatively, expression of mutations in prokaryotic systems would allow demonstration of both activity and stability. Mutations affecting both could lead to secondary disruption of a protein complex, while a stable protein might lead to milder symptoms due to preservation of protein interactions in the complex. Thus, knowledge of the interactive architecture of these proteins in the mitochondria would be useful help predict disease severity. If patient cell lines are not available, modern technologies like CRISPR could be used to create cellular models for analysis. Using CRISPR technology, various disease-causing mutations can be simulated in WT cells. They could then be analyzed for protein-protein interactions by western blotting, proteomic analysis, or STED imaging as for patient cell lines.

My studies show that mutations in the PPA genes lead to accumulation of ROS and that these can be reduced by treatment with a mitochondrial targeted antioxidant. Consistent with this finding, literature studies have reported abnormalities in mitochondrial structure and oxidative phosphorylation. However, there is currently no viable explanation for why this should occur. My results offer one possible solution. The Vockley lab has shown that enzymes of fatty acid oxidation and ETC form a physical complex and that mutations in FAO proteins lead to secondary disruption of oxidative phosphorylation and the accumulation of ROS. Based on my results, I predict that the ILE/VAL metabolic complex interacts with the inner mitochondrial membrane in close approximation to the ETC and TCA cycle in order to promote efficient delivery of propionyl-CoA for energy metabolism. Disruption of such a complex, would destabilize the ETC, and provide one possible pathophysiologic mechanism increased ROS production seen in PPA cells. Stabilization of oxidized cardiolipin by the CLBP would be predicted to stabilize the inner mitochondrial membrane, and thus the ILE/VAL metabolic complex and ETC super-complexes. If this is the case, further STED imaging studies could be performed to analyze a potential interaction between distal members of ILE/VAL catabolism and members of the TCA cycle. To explore this angle further, one could perform STED imaging experiments with and without the treatment of CLBP in the cellular monolayer. An increase in co-localization of BCAA enzymes as well as an increase in co-localization between BCAA enzymes (like PCC and MUT) with TCA cycle or ETC super-complex enzymes would be supportive of important *in vivo* interactions.

Propionyl-CoA is a critical end product of ILE and VAL metabolism, necessary to make succinyl-CoA for the TCA cycle and ETC. The metabolic flux studies performed as part of specific aim 2b led to the relatively surprising discovery that different propiogenic substrates

contributed differentially to the propionylcarnitine pool in cells. Thus, while VAL, MET, ILE and THR are all metabolized at least in part to propionyl-CoA, only the propionyl-CoA from ILE contributes significantly to cellular propionylcarnitine pool. Propionyl-CoA from the other amino acids, presumably find another metabolic destination. This finding has significant clinical implications, namely, that in patients with PPA or MMA, only ILE needs to be restricted in the diet, making dietary management of these patient much easier. As a secondary implication, clinical studies of patients with long chain fatty acid oxidation defects demonstrate a secondary deficiency of the TCA cycle (Figure 5) that is readily reversed by supplementation with odd chain carbon substrates[63]. One might consider BCAAs as an alternate source of TCA cycle intermediates; however, preliminary data by my collaborators at Agios Pharmaceuticals shows that propionyl-CoA derived from labeled ILE does not efficiently enter the TCA cycle (Figure 28). In this experiment, WT human foreskin fibroblast (HFF1) cells were cultured in media containing stably labeled ^{13}C BCAAs. One would expect the incorporation of a BCAA such as ILE to readily enter the TCA cycle through succinyl-CoA; however, little to no ^{13}C labeled malate was detected via MS/MS. This suggests that BCAAs are likely an inadequate treatment for fatty acid oxidation disorders (FAODs).
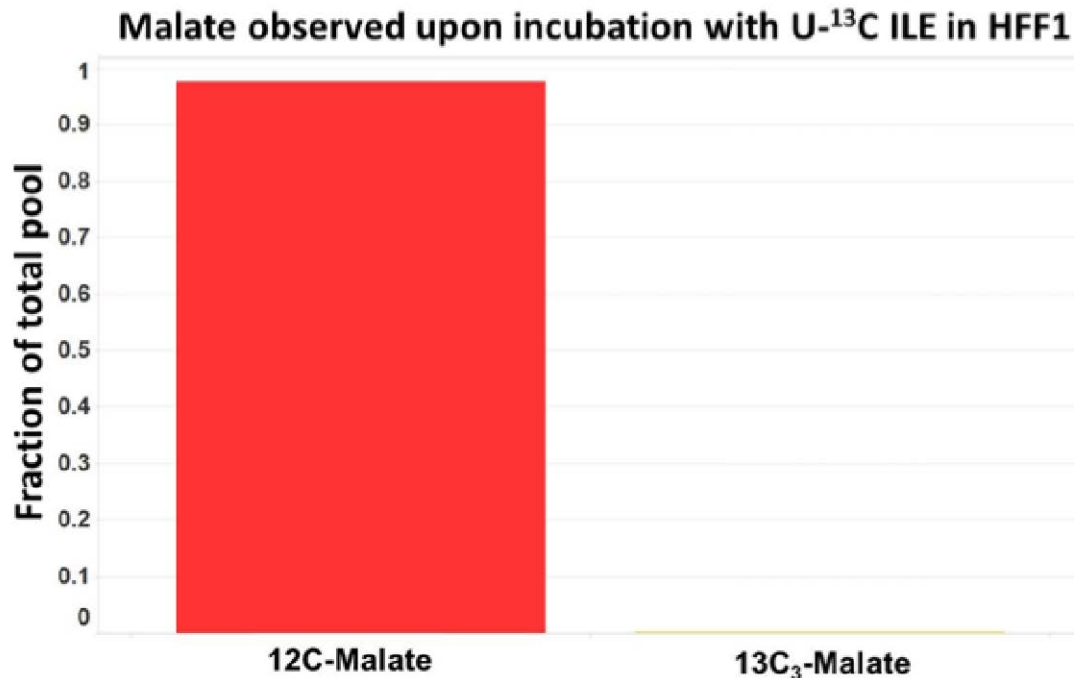
Figure 28. Labeled malate observed upon addition of labeled ILE to WT HFF1 cells.

Of the total measurable malate in the HFF1 cells, little to no labeled metabolite is detected, indicating that propionyl-CoA from ILE does not readily enter the TCA cycle.

Additional experiments are necessary to determine the fate of propionyl-CoA derived from catabolism from VAL, MET, or THR. To test this, cells could be grown in the presence of various labeled amino acids, followed by an analysis by un-targeted metabolomics. I would expect to see an accumulation of labeled propionyl-CoA only in cell lines treated with labeled ILE. Cells treated with VAL, MET, and THR would be more enigmatic, though intermediate metabolites in each of their respective catabolic pathways should be explored to investigate the potential for shunting of these metabolites into other pathways. Additionally, an animal model of PPA or MMA would be useful in studying this hypothesis. Feeding the animals different diets restricted in different combinations of the four labeled "propiogenic" amino acids, followed by

metabolomics analysis as described for cellular experiments would provide additional insight into the fate of propionyl-CoA derived from each amino acid.

While my experimental results are consistent with the presence of one or more BCAA protein complexes, technology has been a major limiting factor. The BCAA metabolic complexes appear to be very labile and were difficult to manipulate *in vitro*. This problem minimized the utility of cross linking and gel electrophoresis experiments. Thus, I eventually switched to a technique that could interrogate interactions *in situ* to minimize the effect of complex instability. In this context, STED generated the most compelling direct evidence of interactions of IVD and 3MCC but not IVD and SBCAD. Unfortunately, lack of availability of appropriate antibodies for these studies limited a more comprehensive exploration of other complex members. As additional antibodies become available, further STED analysis will be possible. Other techniques to directly visualize protein interactions could also be explored. One such technique, immune-electron microscopy, could map the molecular architecture of the BCAA enzymes, potentially using antibodies that were unsuccessful with STED. The lack of stability of BCAA protein complex suggests that it is fluid, *i.e.*, it is not held rigidly in place in the mitochondria, and/or its protein components can change with time. Exploring additional methods to better stabilize this super-complex would allow more robust co-immunoprecipitation proteomic experiments. Finally, it is important to note the limitation of a dearth of patient samples. The branched chain organic acidurias are rare, and a large bank of patient derived cell lines is not available. This was especially true for MMA patient derived cell lines in section 4 above. I had access to two MMA cell lines, but their growth potential and response in metabolic experiments was limited by a high passage number. Once again, gene editing technologies may prove to be crucial to generate appropriate experimental material. Additionally, the study of

more wild type samples will allow assessment of the natural variations in super-complex formation or metabolic flux.

In conclusion, this thesis provides evidence for the presence of a fluid interaction of the enzymes of BCAA into one or more functional protein complexes that likely interacts with the inner mitochondrial membrane. Further, evidence is provided that the contribution of the propiogenic amino acids into the cellular propionylcarnitine pool is unequal and is dominated by ILE. In total, these results provide the opportunity for direct patient benefit by directing development of drugs that improve complex stability and/or abrogate the mitochondrial derangements induced by the lack of complex stability, as well as providing better guidance for the dietary management of disorders of propionate metabolism.

BIBLIOGRAPHY

[1] Knerr I, Weinhold N, Vockley J, Gibson KM. (2012). Advances and challenges in the treatment of branched-chain amino/keto acid metabolic defects. *J Inherit Metab Dis.* **35:**29-40.

[2] Vockley J, Zschocke J, Knerr I, Walsh Vockley C, Gibson KM Branched chain organic acidurias (McGraw-HIll, New York, NY, 2013).

[3] Vockley J, Mohsen AW, Binzak B, Willard J, Fauq A. (2000). Mammalian branched-chain acyl-CoA dehydrogenases: molecular cloning and characterization of recombinant enzymes. *Methods Enzymol.* **324:** 241-58.

[4] Swigonova Z, Mohsen AW, Vockley J. (2009). Acyl-CoA dehydrogenases: Dynamic history of protein family evolution. *Journal of Molecular Evolution.* **69:** 176-93.

[5] Ikeda Y, Dabrowski C, Tanaka K. (1983). Separation and properties of five distinct acyl-CoA dehydrogenases from rat liver mitochondria. *J Biol Chem.* **258:** 1066-76.

[6] Ikeda Y, Tanaka K. (1983). Purification and characterization of isovaleryl Co-enzyme A dehydrogenase from rat liver mitochondria. *J Biol Chem.* **258:** 1077-85.

[7] Ikeda Y, Okamura-Ikeda K, Tanaka K. (1985). Purification and characterization of short-chain, medium-chain, and long-chain acyl-CoA dehydrogenases from rat liver mitochondria. Isolation of the holo- and apoenzymes and conversion of the apoenzyme to the holoenzyme. *J Biol Chem.* **260:** 1311-25.

[8] Ikeda Y, Tanaka K. (1983). Purification and characterization of 2-methyl-branched chain acyl coenzyme A dehydrogenase, an enzyme involved in the isoleucine and valine metabolism, from rat liver mitochondria. *J Biol Chem.* **258:** 9477-87.

[9] Ikeda Y, Tanaka K. (1987). Immunoprecipitation and electrophoretic analysis of four human acyl-CoA dehydrogenases and electron transfer flavoprotein using antibodies raised against the corresponding rat enzymes. *BiochemMedMetabBiol.* **37:** 329-34.

[10] Izai K, Uchida Y, Orii T, Yamamoto S, Hashimoto T. (1992). Novel fatty acid b-oxidation enzymes in rat liver mitochondria. 1. Purification and properties of very-long-chain acyl-coenzyme A dehydrogenase. *J Biol Chem.* **267:** 1027-33.

[11] Rozen R, Vockley J, Zhou L, Milos R, Willard J, Fu K, Vicanek C, Low-Nang L, Torban E, Fournier B. (1994). Isolation and expression of a cDNA encoding the precursor for a novel member (ACADSB) of the acyl-CoA dehydrogenase gene family. *Genomics.* **24:** 280-7.

[12] Willard J, Vicanek C, Battaile KP, Van Veldhoven PP, Fauq AH, Rozen R, Vockley J. (1996). Cloning of a cDNA for short/branched chain acyl-Coenzyme A dehydrogenase from rat and characterization of its tissue expression and substrate specificity. *Arch Biochem Biophys.* **331:** 127-33.

[13] Nguyen TV, Andresen BS, Corydon TJ, Ghisla S, Abd-El Razik N, Mohsen AW, Cederbaum SD, Roe DS, Roe CR, Lench NJ, Vockley J. (2002). Identification of isobutyryl-CoA dehydrogenase and its deficiency in humans. *Mol Genet Metab.* **77:** 68-79.

[14] Zhang J, Zhang W, Zou D, Chen G, Wan T, Zhang M, Cao X. (2002). Cloning and functional characterization of ACAD-9, a novel member of human acyl-CoA dehydrogenase family. *Biochem Biophys Res Commun.* **297:** 1033-42.

[15] Blackburn PR, Gass JM, Vairo FPE, Farnham KM, Atwal HK, Macklin S, Klee EW, Atwal PS. (2017). Maple syrup urine disease: mechanisms and management. *Appl Clin Genet.* **10**: 57-66

[16] Sitta A, Ribas GS, Mescka CP, Barschak AG, Wajner M, Vargas CR. (2014). Neurological damage in MSUD: the role of oxidative stress. *Cell Mol Neurobiol.* 34(2): 157-65.

[17] Tanaka K, Budd MA, Efron ML, Isselbacher KJ. (1966). Isovaleric acidemia: a new genetic defect of leucine metabolism. *Proc Natl Acad Sci USA.* **56:** 236-42.

[18] Budd MA, Tanaka K, Holmes LB, Efron ML, Crawford JD, Isselbacher KJ. (1967). Isovaleric acidemia-clinical features of a new genetic defect of leucine metabolism. *NEnglJMed.* **277:** 321-.

[19] Elsas LJ, 2nd, Naglak M. (1988). Acute and chronic-intermittent isovaleric acidemia: diagnosis and glycine therapy. *Acta Paediatr Jpn.* **30:** 442-51.

[20] Levy HL, Erickson AM, Lott IT, Kurtz DJ. (1973). Isovaleric acidemia: results of family study and dietary treatment. *Pediatrics.* **52:** 83-94.

[21] Lott IT, Erickson AM, Levy HL. (1972). Dietary treatment of an infant with isovaleric acidemia. *Pediatrics.* **49:** 616-8.

[22] Efron ML. (1967). Isovaleric acidemia. *American Journal of Diseases of Children.* **113:** 74-6.

[23] Grunert SC, Wendel U, Lindner M, Leichsenring M, Schwab KO, Vockley J, Lehnert W, Ensenauer R. (2012). Clinical and neurocognitive outcome in symptomatic isovaleric acidemia. *Orphanet J Rare Dis.* **7:** 9.

[24] Gibson KM, Burlingame TG, Hogema B, Jakobs C, Schutgens RBH, Millington D, Roe CR, Roe DS, Sweetman L, Steiner RD, Linck L, Pohowalla P, Sacks M, Kiss D, Rinaldo P, Vockley J. (2000). 2-Methylbutyryl-coenzyme A dehydrogenase deficiency: A new inborn error of L-isoleucine metabolism. *Pediatric Research.* **47:** 830-3.

[25] Matern D, He M, Berry SA, Rinaldo P, Whitley CB, Madsen PP, van Calcar SC, Lussky RC, Andresen BS, Wolff JA, Vockley J. (2003). Prospective diagnosis of 2-methylbutyryl-CoA dehydrogenase deficiency in the Hmong population by newborn screening using tandem mass spectrometry. *Pediatrics.* **112:** 74-8.

[26] van Calcar SC, Gleason LA, Lindh H, Hoffman G, Rhead W, Vockley G, Wolff JA, Durkin MS. (2007). 2-methylbutyryl-CoA dehydrogenase deficiency in Hmong infants identified by expanded newborn screen. *Wisconsin Medical Journal.* **106:** 12-5.

[27] Roe CR, Cederbaum SD, Roe DS, Mardach R, Galindo A, Sweetman L. (1998). Isolated isobutyryl-CoA dehydrogenase deficiency: An unrecognized defect in human valine metabolism. *Molecular Genetics & Metabolism.* **65:** 264-71.

[28] Koeberl DD, Young SP, Gregersen N, Vockley J, Smith WE, Benjamin DK, An Y, Weavil SD, Chaing SH, Bali D, McDonald MT, Kishnani PS, Chen YT, Millington DS. (2003). Rare disorders of metabolism with elevated butyryl- and isobutyryl-carnitine detected by tandem mass spectrometry newborn screening. *Pediatric Research.* **54:** 219-23.

[29] Sass JO, Sander S, Zschocke J. (2004). Isobutyryl-CoA dehydrogenase deficiency: isobutyrylglycinuria and ACAD8 gene mutations in two infants. *J Inherit Metab Dis.* **27:** 741-5.

[30] Oglesbee D, He M, Majumder N, Vockley J, Ahmad A, Angle B, Burton B, Charrow J, Ensenauer R, Ficicioglu CH, Keppen LD, Marsden D, Tortorelli S, Hahn SH, Matern D. (2007). Development of a newborn screening follow-up algorithm for the diagnosis of isobutyryl-CoA dehydrogenase deficiency. *Genet Med.* **9:** 108-16.

[31] Mohsen AW, Vockley J. (2015). Kinetic and Spectral Properties of Isovaleryl-CoA Dehydrogenase and Interaction with Ligands. *Biochemie*. **108**: 108-119.

[32] Battaile KP, Nguyen TV, Vockley J, Kim JP. (2004). Structures of Isobutyryl-CoA Dehydrogenase and Enzyme-Product Complex Comparison with Isovaleryl- And Short-Chain Acyl-CoA Dehydrogenases. *J Biol Chem*. **279**: 16526-34.

[33] He M, Burghardt TP, Vockley J. (2003). A Novel Approach to the Characterization of Substrate Specificity in Short/Branched Chain Acyl-CoA Dehydrogenase. J Biol Chem. 278: 37974-86.

[34] Liu X, Wu L, Deng G, Chen G, Li N, Chu X, Li D. (2013). Comparative studies of Acyl-CoA dehydrogenases for monomethyl branched chain substrates in amino acid metabolism. *Bioorg Chem*. **47**: 1-8.

[35] Lau EP, Cochran BC, Fall RR. (1980). Isolation of 3-methylcrotonyl-coenzyme A carboxylase from bovine kidney. *Arch Biochem Biophys*. **205**: 352.

[36] Stadler SC, Polanetz R, Maier EM, Heidenreich SC, Niederer B, Mayerhofer PU, Lagler F, Koch HG, Santer R, Fletcher JM, Ranieri E, Das AM, Spiekerkotter U, Schwab KO, Potzsch S, Marquardt I, Hennermann JB, Knerr I, Mercimek-Mahmutoglu S, Kohlschmidt N, Liebl B, Fingerhut R, Olgemoller B, Muntau AC, Roscher AA, Roschinger W. (2006). Newborn screening for 3- methylcrotonyl-CoA carboxylase deficiency: population heterogeneity of MCCA and MCCB mutations and impact on risk assessment. *Hum Mutat*. **27**, 748-759.

[37] Wongkittichote P, Mew NA, Chapman KA. (2017). Propionyl-CoA carboxylase – a review. *Mol Genet Metab*. 122(**4**): 145-152.

[38] Pena L, Franks J, Chapman KA, Gropman A, Ah MN, Chakrapani A, Island E, MacLeod E, Matern D, Smith B, Stagni K, Sutton VR, Ueda K, Urv T, Venditti C, Enns GM, Summar ML. (2012). Natural history of propionic acidemia. *Mol Genet Metab*. **105**: 5-9.

[39] Darvish-Damavandi M, Ho HK, Kang TS. (2016). Towards the development of an enzyme replacement therapy for the metabolic disorder propionic acidemia. *Met Genet Metab Rep*. **8**: 51-60.

[40] Tuncel AT, Boy N, Morath MA, Horster F, Mutze U, Kolker S. (2018). Organic acidurias in adults: late complications and management. J Inherit Metab Dis. 10.1007/s10545-017-0135-2.

[41] Hackenbrock C.R., Chazotte B., Gupte S.S. (1986). The random collision model and a critical assessment of diffusion and collision in mitochondrial electron transport. *J. Bioenerg. Biomembr*. **18**:331–368.

[42] Genova M.L., Lenaz G. (2014). Functional role of mitochondrial respiratory supercomplexes. *Biochim. Biophys. Acta*. **1837**:427–443.

[43] Leiptnitz G, Mohsen AW, Karunanidhi A, Seminotti B, Roginskaya VY, Markantone DM, Grings M, Mihalik SJ, Wipf P, Van Houten P, Vockley J. (2018). Evaluation of mitochondrial bioenergetics, dynamics, endoplasmic reticulum-mitochondria crosstalk,

and reactive oxygen species in fibroblasts from patients with complex I deficiency. *Sci Rep*. 8(**1**): 1165.

[44] El-Hattab AW, Zarante AM, Almannai M, Scaglia F. (2017). Therapies for mitochondrial diseases and current clinical trials. *Mol Genet Metab*. 122(**3**): 1-9.

[45] Villani GR, Gallo G, Scolamiero E, Salvatore F, Ruoppolo M. (2017). "Classical organic acidurias": diagnosis and pathogenesis. Clin Exp Med. 17(3): 305-323.

[46] Tanaka K, Budd MA, Efron ML, Isselbacher KJ. (1966). Isovaleric acidemia: a new genetic defect of leucine metabolism. *Proc Natl Acad Sci USA*. **56**:236-242.

[47] Ren M, Phoon CKL, Schlame M. (2014). Metabolism and function of mitochondrial cardiolipin. *Prog Lipid Res*. **55**: 1-16.

[48] Musatov A, Sedlák E. (2017). Role of cardiolipin in stability of integral membrane proteins. *Biochemie*. **17**: 30222-5.

[49] Shevchenko A, Tomas H, Havlis J, Olsen JV, Mann M. (2006). In-gel digestion for mass spectrometric characterization of proteins and proteomes. *Nat Protoc*. 1(**6**): 2856-2860.

[50] Granvogl B, Gruber P, Eichacker LA. (2007). Standardisation of rapid in-gel digestion by mass spectrometry. *Proteomics*. 7(**5**): 642-54.

[51] Granvogl B, Plöscher M, Eichacker LA. (2007). Sample preparation by in-gel digestion for mass spectrometry-based proteomics. *Anal Bioanal Chem*. 389(**4**): 991-1002.

[52] Hein B, Willig KI, Hell SW. (2008). Stimulated emission depletion (STED) nanoscopy of a fluorescent protein-labeled organelle inside a living cell. *Proc Natl Acad Sci*. 105(**38**): 14271-76.

[53] Westphal V, Rizzoli SO, Lauterbach MA, Kamin D, Jahn R, Hell SW. (2008). Video-rate far-field optical nanoscopy dissects synaptic vesicle movement. *Science*. **320**: 246-9.

[54] Ishigaki M, Iketani M, Sugaya M, Takahashi M, Tanaka M, Hattori S, Ohsawa I. (2016). STED super-resolution imaging of mitochondria labeled with TMRM in living cells. *Mitochondrion*. **28**:79-87.

[55] Lu W, Clasquin MF, Melamud E, Amador-Noguez D, Caudy AA, Rabinowitz JD. (2010). Metabolomic analysis via reversed-phase ion-pairing liquid chromatography couple to a stand alone orbitrap mass spectrometer. *Anal Chem*. 82(**8**):3212-21.

[56] Vockley J, Rogan PK, Anderson BD, Willard J, Seelen RS, Smith DI, Liu W. (200). Exon Skipping in IVD RNA Processing in Isovaleric Acidemia Caused by Point Mutations in the Coding Region of the *IVD* Gene. *Am J Hum Genet*. 66(**2**):356-67.

[57] Pedersen CB, Bischoff C, Christensen E, Simonsen H, Lund AM, Young SP, Koeberl DD, Millington DS, Roe CR, Roe DS, Wanders RJ, Ruiter JP, Keppen LD, Stein Q, Knudsen I, Gregersen N, Andresen BS. (2006). Variations in IBD (ACAD8) in children with elevated C4-carnitine detected by tandem mass spectrometry newborn screening. *Pediatr Res*. 60(**3**): 315-20.

[58] Alfardan J, Mohsen AW, Copeland S, Ellison J, Keppen-Davis L, RohrbachM, Powell BR, Gillis J, Matern D, Kant J, Vockley J. (2010). Characterization of new ACADSB gene sequence mutations and clinical implications in patients with 2-methylbutyrylglycinuria identified by newborn screening. *Mol Genet Metab*. 100(**4**): 333-8.

[59] Claypool, S.M., Boontheung, P., McCaffery, J.M., Loo, J.A., Koehler, C.M. (2008). The cardiolipin transacylase, tafazzin, associates with two distinct respiratory components providing insight into Barth syndrome. *Mol Biol Cell*. **19:** 5143-5155.

[60] Wu J, Hao S, Sun XR, Zhang H, Li H, Zhao H, Ji MH, Yang JJ, Li K. (2017). Elamipretide (SS-31) Ameliorates Isoflurane-Induced Long-Term Impairments of Mitochondrial Morphogenesis and Cognition in Developing Rats. *Front Cell Neurosci*. **11**: 119.

[61] Ledley FD, Crane AM, Lumetta M. (1990). Heterogeneous alleles and expression of methylmalonyl CoA mutase in mut methylmalonic acidemia. *Am J Hum Genet*. **46**:539-47.

[62] He M, Burghardt TP, Vockley J. (2003). A Novel Approach to the Characterization of Substrate Specificity in Short/Branched Chain Acyl-CoA Dehydrogenase. *J Biol Chem*. **278**: 37974-86.

[63] Vockley J, Marsden D, McCracken E, DeWard S, Barone A, Hsu K, Kakkis E. (2015). Long term major clinical outcomes in patients with long chain fatty acid oxidation disorders before and after transition to triheptanoin treatment—A retrospective chart review. *Mol Genet Metab*. **116**(1-2): 53-60.